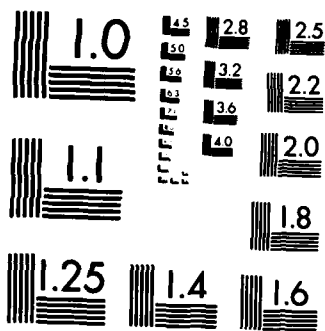END

FILMED

DTIC

MICROCOPY RESOLUTION TEST CHART

NATIONAL BUREAU OF STANDARDS-1963-A

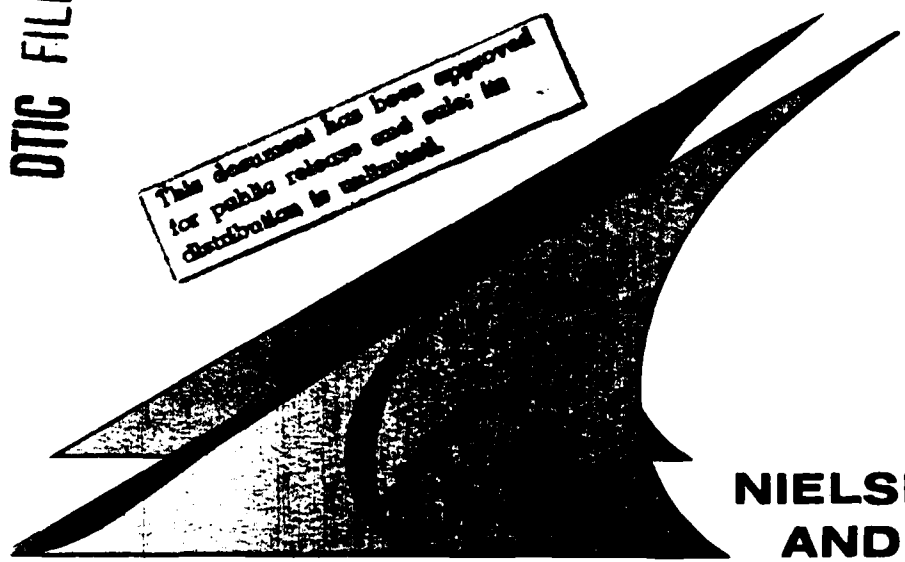# COMPUTATIONAL MODELS OF THE VISCOUS SUBLAYER AND LIMITING BEHAVIOR OF TURBULENCE NEAR A WALL

by

Dean R. Chapman and Gary D. Kuhn

NIELSEN ENGINEERING AND RESEARCH, INC.

COMPUTATIONAL MODELS OF THE VISCOUS SUBLAYER AND LIMITING BEHAVIOR OF TURBULENCE NEAR A WALL

by

Dean R. Chapman and Gary D. Kuhn

NEAR TR 334
December 1984

DTIC
ELECTE
MAR 1 4 1985
S
E
D

NIELSEN ENGINEERING & RESEARCH, INC.
510 Clyde Avenue, Mountain View, CA   94043
(415) 968-9457

REPORT DOCUMENTATION PAGE	READ INSTRUCTIONS BEFORE COMPLETING FORM

1. REPORT NUMBER	2. GOVT ACCESSION NO.	3. RECIPIENT'S CATALOG NUMBER
	AD-A151 198	

4. TITLE (and Subtitle)	5. TYPE OF REPORT & PERIOD COVERED
Computational Models of the Viscous Sublayer and Limiting Behavior of Turbulence Near a Wall	Final Report 15 July, 1982-30 Sept, 1984
	6. PERFORMING ORG. REPORT NUMBER
	NEAR TR 334

7. AUTHOR(s)	8. CONTRACT OR GRANT NUMBER(s)
Dean R. Chapman Gary D. Kuhn	N00014-82-C-0672

9. PERFORMING ORGANIZATION NAME AND ADDRESS	10. PROGRAM ELEMENT, PROJECT, TASK AREA & WORK UNIT NUMBERS
NIELSEN ENGINEERING & RESEARCH, INC. 510 Clyde Avenue, Mountain View. CA 94043	

11. CONTROLLING OFFICE NAME AND ADDRESS	12. REPORT DATE
OFFICE OF NAVAL RESEARCH Arlington, VA 22217	December, 1984
	13. NUMBER OF PAGES
	66 pages

14. MONITORING AGENCY NAME & ADDRESS(if different from Controlling Office)	15. SECURITY CLASS. (of this report)
	Unclassified
	15a. DECLASSIFICATION DOWNGRADING SCHEDULE

16. DISTRIBUTION STATEMENT (of this Report)

Approved for public release.
Distribution unlimited.

17. DISTRIBUTION STATEMENT (of the abstract entered in Block 20, If different from Report)

18. SUPPLEMENTARY NOTES

19. KEY WORDS (Continue on reverse side if necessary and identify by block number)

Turbulence
Viscous Sublayer

20. ABSTRACT (Continue on reverse side if necessary and identify by block number)

· Three computational models of incompressible viscous sublayer turbulence have been developed using the time-dependent Navier-Stokes equations with prescribed velocity boundary conditions at the outer edge of the sublayer. The models attempt in different ways to simulate the highly elongate, quasi-periodic, coherent structures observed experimentally. Comparison of computed results with experiment is good for mean

DD FORM 1 JAN 73 1473

streamwise velocity, mean Reynolds stress, and correlation coefficient; and reasonably good for the three turbulence intensities, Reynolds stress intensity, skewness and flatness of streamwise velocity and of Reynolds stress. Within a thin layer adjacent to the outer edge, all three models yield anomalously high values for dissipation and streamwise vorticity intensity.

Computations using a fine mesh establish the limiting behavior of turbulence quantities very near a wall. Below about 0.3 wall units, the variations with distance from the wall were found to be: linear for streamwise turbulence, spanwise turbulence, and the departure of dissipation and streamwise vorticity from their wall values; second power for turbulence normal to the wall; third power for Reynolds stress; and a constant non-zero value for the correlation coefficient. A simple physical explanation involving mass conservation in sweep and ejection events is given for the third-power variation of Reynolds stress in streamwise homogeneous as well as in-homogeneous flows. Application is made to Reynolds average turbulence modeling to derive proper damping functions for Reynolds stress in eddy-viscosity models, and three new wall boundary conditions for dissipation in k-ε and stress equation models.

NOTATION

a_n, b_n Coefficients of Fourier series for intermittent pulse function, Eq. (10)-(13).

A Constant in damping factor.

C Correlation coefficient in random number sequence.

D Damping factor for Reynolds stress.

F Flatness factor $\langle(\ \ )^4\rangle/\langle(\ \ )^2\rangle^2$; also intermittent pulse function (Eq. 8 and 9).

F_i Body force.

H Intermittent pulse function, Eq. (10).

I_t Integral time scale of turbulence

k Turbulence kinetic energy

LSE   Large scale eddy

M Number of terms in Fourier series

MSE   Medium scale eddy

n Frequency

N Frequency in wall variables

p Pressure

P Pressure in wall variables

R_e Reynolds number

R_{uv} Correlation coefficient $\langle uv\rangle/(\langle u^2\rangle\langle v^2\rangle)^{1/2}$

$R_{u2}, R_{v3}, R_{w3}, R_n$ Random sequences, Eq. (14) and 28)

S Skewness $\langle(\ \ )^3\rangle/\langle(\ \ )^2\rangle^{3/2}$.

S'_x, S'_z Fluctuation intensity of streamwise spanwise wall shear stress.

SSE   Small scale eddy

t Time

T Time in wall variables

u_τ	Friction velocity $\sqrt{\langle \tau_w \rangle / \rho}$
u, v, w	Fluctuating velocity components
U_i	Total velocity components, $\langle U_i \rangle + u_i$; $i = 1, 2, 3$ corresponds to x, y and z components of velocity
x, y, z	Length coordinates
X, Y, Z	Length coordinates in wall variables
X_1, X_2	Parameters appearing in intermittent pulse function (Eq. 12 and 13)
α, β, γ	rms turbulence intensities streamwise, normal, spanwise at outer edge of viscous sublayer
δ	boundary layer thickness or channel half height
ϵ	rate of turbulent dissipation
λ	mean spanwise spacing between streaks
ν	kinematic viscosity
ρ	density
σ	variance of random number sequence
τ	shear stress
ζ	spanwise coordinate $2\pi Z/\lambda$
θ	momentum thickness
ϕ	phase angle

SUBSCRIPTS

+	wall variables (Eq. 3 and foot note on page 11)
1	small scale eddies
2	large scale eddies
3	medium scale eddies
e	edge of viscous sublayer
es	ejection/sweep event
op	oscillating plate flow
os	oscillating shear flow
ppa	peak to peak amplitude
∞	edge of boundary layer or channel mid-point
w	wall
x	refers to x direction
z	refers to z direction

Special Notation

( )'	rms fluctuation about mean value
< >	space-time mean for computations, time mean for experiments
$\overline{(\quad)}$	time mean at a fixed point

TABLE OF CONTENTS

INTRODUCTION

The modeling of near-wall turbulence represents one of the weak links in present computational methods for wall-bounded flows. Turbulence production, dissipation and kinetic energy reach their maxima within the extremely thin viscous sublayer adjacent to a wall. Because of this thinness it has not been technically feasible to measure in the variety of flows of practical interest some of the most important elements involved in turbulence modeling - such as dissipation rate and the limiting near-wall behaviour. Such circumstances have restricted significantly the accuracy of present turbulence models.

The objective of the present research is to explore use of the time-dependent Navier-Stokes equations as a method of modeling viscous sublayer turbulence. This method attempts to model directly the experimental observations of highly-elongate organized eddy structures near a wall. Such modeling is not limited as experiments are by the extreme thinness of the viscous sublayer, but is limited by the degree to which realism can be built into the boundary conditions for Navier-Stokes equations. These boundary conditions, to be realistic, must represent the main physical features of both organized structures and disorganized turbulence.

One of the principal motivations for this research is the possibility of providing a basis for strengthening present Reynolds-average closure schemes. Because the modeled differential equations for free turbulence yield demonstrably incorrect results near a wall, various ad hoc functions (up to 5 in number for k- ε methods) are conventionally added in an effort to mend this shortcoming. Without a sound guide from experiment, the inevitable consequence has been that different models with

different ad hoc functions have yielded different results (Patel et. al 1981). If, however, Navier-Stokes computations could provide an improved guide to the modeling, then conventional turbulence models might be strengthened. A further motivation for the research undertaken is the possibility of producing a simple test flow against which various subgrid scale models of turbulence in large eddy simulations might be tested.

The method used herein to model turbulence is termed "coherent-structure" modeling. It differs from conventional Reynolds-averaged methods in that it overtly attempts to model organized quasi-periodic eddy structures in the sublayer. Since the process of Reynolds averaging obliterates at the outset much of the physics of organized motion, it has not been possible to incorporate such features in the framework of Reynolds-average modeling. The conventional procedure is to first time-average the dynamic equations, then model turbulence transport terms, and finally compute results. In contradistinction, we first model turbulent velocity boundary conditions, then compute time-dependent dynamics, and finally time-average results. Thus, time-averaging is the last operation performed on computed dynamics, rather than the first operation performed on dynamic equations.

In recent years several coherent-structure models of viscous sublayer turbulence have been explored. An initial model of Hatziavramidis and Hanratty (1979) used extremely simplified boundary conditions and obtained some interesting qualitative features, although the results were not quantitatively realistic in important respects (e.g. yielding zero Reynolds stress and zero turbulence intensity at the outer edge of the viscous sublayer). Subsequent coherent-structure models of Chapman and Kuhn (1981) and of Nikolaides and Hanratty (1983) have employed somewhat more sophisticated boundary conditions in representing

the coherent structures, and have yielded more realistic results. One unrealistic aspect of these models, however, is that they produce anomalously high values for dissipation near the outer edge of the viscous sublayer (Kaneda and Leslie (1982)). Because dissipation is a key quantity modeled in Reynolds-average closure schemes, considerable attention is given in the present research to this anomaly.

Three different coherent-structure models are explored herein. They differ mainly in the complexity of the space-and time dependent boundary conditions imposed on the Navier-Stokes equations at the outer edge of the viscous sublayer. The first model uses simple harmonically varying components of velocity to simulate large-scale and small-scale eddies. The second model adds complexity by simulating time-intermittent production c Reynolds-stress, and by including a third velocity component to simulate intermediate-scale eddies. The third model adds a further element of complexity by using randomly generated time functions in place of harmonic variations. All of the models are restricted to incompressible flow without heat transfer. The mathematical development includes the effects of a mean streamwise pressure gradient, although comparisons with experimental data are made herein only for zero or small pressure gradients.

EXPERIMENTAL OBSERVATIONS GUIDING MODEL FORMULATION

The key technical step in model development is to construct appropriate boundary conditions for the three fluctuating velocity components at the outer edge of the viscous sublayer (VSL). An attempt is made to formulate these so as to reflect as well as possible the main organized motions delineated by experiments. Seven principal observational features of coherent sublayer structure have been selected as guidelines for the velocity boundary conditions to emulate, as listed in the paragraphs which follow.

1. Relatively Small Scale Eddies (SSE) produce the principal Reynolds stress. Near the outer edge of the VSL, Kim, et al (1971) observed "ejection" events involving $u < 0$ and $v > 0$ which contribute about 70% to $\overline{uv}$, and "sweep" events involving $u > 0$ and $v < 0$ which contribute about 60%, while other interactions contribute negatively about 30% according to Wallace, et al (1972). Characteristic spanwise dimensions of these stress producing eddies are small, being about 10 to 30 wall units (Lu and Willmarth, 1973; Kline et al, 1967; and Corino and Brodkey, 1969). At high Re these dimensions are the order of $10^{-2} \delta$ to $10^{-3} \delta$. Thus, relatively small-scale eddies must be treated in modeling VSL turbulence.

2. Organized Large Scale Eddies (LSE) exist in the region external to the VSL (Kovasnay et al, 1970; Falco, 1977; Brown and Thomas, 1977). Their mean period determined from streamwise autocorrelation data is $T_{LSE} \simeq 5\delta/U_\infty$, independent of Re (Badri Narayanan and Marvin, 1978). Because LSE interact with the SSE, their effects must also be included in the computational model.

-4-

In summary, Model 2 differs from Model 1 in several ways: it simulates intermittent bursting and Reynolds stress production, rather than sinusoidal as in Model 1; it employs a medium-scale eddy component for v_e, whereas Model 1 has none; and it also employs a medium-scale eddy component for w_e whereas Model 1 employs a large-scale component. A further difference is that Model 2 does not employ a body pressure gradient term associated with the large scale eddy component for u.

Model 3

The primary feature characterizing Model 3 is the use of time functions for LSE and MSE that are randomly generated instead of harmonic. Otherwise it is similar to Model 2. The periodic small-scale eddy structure remains the same as in Model 2. The outer edge boundary conditions for Model 3 are

SSE	LSE	MSE
Scale λ	Scale $> 10\ \lambda$	Scale 3λ

$$u_e = \sqrt{2}\ \alpha_1 F_u(N_1 T)\ \sin\zeta \qquad \alpha_2 R_{u2}(T)$$

$$v_e = \sqrt{2}\ \beta_1 F_u(N_1 T)\ \sin\zeta \qquad\qquad\qquad \sqrt{2}\ \beta_3 R_{v3}(T)\ \sin\frac{\zeta}{3} \qquad (14)$$

$$w_e = \sqrt{2}\ \gamma_1 F_w(N_1 T)\ \cos\zeta \qquad\qquad\qquad \sqrt{2}\ \gamma_3 R_{w3}(T)\ \cos\frac{\zeta}{3}$$

ORDER   DISORDER

where the three functions $R_{u2}(T)$, $R_{v3}(T)$, $R_{w3}(T)$ are random functions of time, each independently generated, and each normalized to have an rms value of unity. All constants N_1, α_1, α_2, β_1, β_2, γ_1, and γ_2 are the same as in Model 2. The essential difference from Model 2, therefore, is that Model 3 simulates disorder in the LSE and MSE, whereas Model 2 simulates relatively coherent harmonic order in these eddies.

These results would suggest a value of β_1/β between 0.49 and 0.72. For simplicity $\beta_1/\beta = 1/\sqrt{2} = .707$ is used in the numerical computations. This corresponds to equal amounts of v^2 energy in small-scale and medium-scale eddies. From the correlation-coefficient equation it follows that $\alpha_1/\alpha = .635$.

The value of γ_1/γ was determined by computer trial to yield a relatively smooth curve for $w'(Y)$. In runs with only the SSE active, it was found that various prescribed values of γ_1 would result in substantially the same level of $(w') \approx 0.45$ over much of the sublayer. Hence, $\gamma_1 = 0.45$ was selected as the outer edge turbulence intensity of the SSE for Model 2.

The frequency N_{u2} of the large scale eddies is taken to be the same as in Model 1, namely, that given by equation (6). As in Model 1, numerical computations for Model 2 have been made for $N_{u2} = N_1 = 0.44$, corresponding to a Reynolds number of $Re_\delta \approx 14,000$.

The frequencies N_{v3} and N_{w3} were taken to be equal. In most calculations for model 2 they were taken to be $N_{v3}=N_{w3}=3N_1$.

In the numerical computations for Model 2 a body pressure gradient is not imposed in association with the large scale eddies. This feature differs from Model 1. Computer runs for Model 2 were made both with and without the body pressure gradient term. The results were somewhat better without this term, although the differences were not major.

5th-order polynominal. It is noted that $\phi_{w1} = 25.8°$ corresponds to the SSE pulse in w leading in time the corresponding ejection/sweep pulses of u and v.

The $(uv)_e$ correlation coefficient for the above boundary conditions is $-(R_{uv})_e = \alpha_1 \beta_1/\alpha\beta$, which is set equal to 0.45. The ratio β_1/β is evaluated from peak-to-peak ratios in conditional samples of the ejection/sweep event taken from either experiments or from large eddy simulations. Two different methods of evaluations have been explored:

1. Equating the peak-to-peak amplitude ratio $\langle v \rangle_{ppa}/\langle u \rangle_{ppa}$ to β_1/α_1, and then using the above equation for $(R_{uv})_e$ to determine both β_1/β and α_1/α;

2. Equating measured values of the fraction of total u^2 energy during bursts to α_1/α, and then using the $(R_{uv})_e$ equation to determine β_1/β.

Results of these determinations are as follows with square brackets designating conditional samples:

Data Source	Method	β_1/β
Chen & Blackwelder (1978)	[v]/[u] plus $R_{uv} = -0.45$	0.53
Nakagawa & Nezu (1981)	[v]/[u] plus $R_{uv} = -0.45$	0.72
Blackwelder & Kaplan (1976)	[v]/[u] plus $R_{uv} = -0.45$	0.49
Kim (1983)	[v]/[u] from LES computations, plus $R_{uv} = -0.45$	0.60
Kim, Kline, & Reynolds (1971)	Fraction of total u^2 energy during bursts (0.68), plus $R_{uv} = -0.45$	0.59
Blackwelder & Kaplan (1976)	[v]/[u] plus $R_{uv} = -0.45$	0.64

where T = time in wall variables, and

N_1 = frequency of ejection/sweep events

N_{u2} = $2\pi U_\infty/5\delta$ = frequency of large-scale eddies

N_{v3}, N_{w3} = frequency of medium-scale eddies

ζ = $2\pi Z/\lambda$

ϕ = $N_1 T$

$$-F_u(\phi) = F_v(\phi) = \frac{H(\phi)}{\overline{H^2(\phi)}} \qquad (9)$$

$$F_w(\phi) = -\frac{H(\phi + \phi_{w_1})}{\overline{H^2(\phi + \phi_{w_1})}}$$

The function $H(\phi)$ is formed by the first M terms of a fourier series for the intermittent rectangular pulse function sketched in figure 2.

$$H(\phi) = \sum_1^M [a_n \cos(n\phi) + b_n \sin(n\phi)] \qquad (10)$$

$$\overline{H^2(\phi)} = \frac{1}{2} \sum_1^M (a_n^2 + b_n^2) \qquad (11)$$

$$a_n = \frac{1}{\pi n} [\sin(nX_1) - \frac{X_1}{X_2} \sin(nX_2)] \qquad (12)$$

$$b_n = \frac{1}{\pi n} \{\frac{X_1}{X_2} [\cos(nX_2)-1] + [\cos(nX_1)-1]\} \qquad (13)$$

values of M between 3 and 5, and values of $X_1 \neq X_2$ have been investigated with little difference in computed results. For the results presented herein, M = 5 and $X_1 = X_2 = 0.3$. The phase angle ϕ_{u2} = 60° was determined by computer trial, as in model 1, to yield a reasonable level for the skewness of u. The phase angle ϕ_{w1} = 25.8° was mathematically determined, also as in Model 1, by the requirement that $(\partial \overline{v^2}/\partial Y)_e = 0$. Since M=5, this particular determination involved solving for the roots of a

have been obtained by Fulachier (1972) at y-values near the outer edge of the viscous sublayer. Spectral parameters at Y = 40, interpolated between his measurements at Y = 31 and 77, are shown in figure 1 wherein k represents the wave number, and f the spectral density. Since

$$\int_O^\infty fdk = \int_O^\infty kfd(\ln k) = 1 \tag{7}$$

the areas under the curves of u^2kf_u, v^2kf_v, and w^2kf_w versus log (k) are proportional to the relative amounts of kinetic energy in these velocity components. The two dashed lines shown along the k axis correspond to large eddies of scale π/δ (where δ is the boundary layer thickness) and to small eddies of scale π/λ. The Reynolds-stress producing SSE, of course, must be included for all three velocity components. If only a second component is selected, the spectral data suggest that the most appropriate such component would be a large scale eddy for u, and medium-scale eddies (MSE) for v and w. In contradistinction to the structure of Model 1, these spectral data do not indicate the presence of a major LSE component for w. Thus the boundary conditions for Model 2 are structured to represent SSE and LSE for u_e, coupled with SSE and MSE for v_e and w_e. The latter MSE are structured to be out of phase in both space and time in order to yield $\overline{uw} = 0$ throughout the sublayer.

SSE	LSE	MSE
Scale λ	Scale $> 10\lambda$	Scale 3λ

$$u_e = \sqrt{2}\,\alpha_1 F_u(\phi)\sin\zeta \qquad +\sqrt{2}\alpha_2\sin(N_{u2}T + \phi_{u2})$$

$$v_e = -\sqrt{2}\beta_1 F_v(\phi)\sin\zeta \qquad\qquad + 2\beta_3\sin(N_{v3}T)\sin\tfrac{1}{3}\zeta$$

$$w_e = \sqrt{2}\gamma_1 F_w(\phi)\cos\zeta \qquad\qquad + 2\gamma_3\cos(N_{w3}T)\cos\tfrac{1}{3}\zeta$$

model 1 differ somewhat from those of Chapman and Kuhn who used $N_1 = .025$, $\phi_{w_2} = 3\pi/4$ and $\phi_{u_2} = \pi/3$, but otherwise used the same constants.

The LSE frequency N_{u2} is determined by the mean period $\overline{T}_{LSE}$ of organized large scale eddies as obtained from the experimental relationship $U_\infty \overline{T}_{LSE} \simeq 5\delta$. Since $N_{u2} \overline{T}_{LSE} = 2\pi$, the large-eddy frequency is

$$N_{u2} = \frac{2\pi U_\infty}{5\delta} \tag{6}$$

which is Reynolds-number dependent. For a flat plate or channel flow the dependence of N_{u2} on Re is as follows

Re_δ	δ_+	R_θ	N_{u2}
4700	240	460	.1
11500	530	1100	.05
29000	1200	2800	.025
67000	2500	6500	.0125
160000	5600	15600	.00625

For simplicity, numerical computations herein have been made for $N_{u2} = N_1 = .044$. This corresponds to a Reynolds number of $Re_\delta \simeq 14,000$.

Model 2

Relative to Model 1, this model adds complexity by structuring the velocity boundary conditions to simulate intermittent production of burst events and hence of Reynolds stress. Also, two components of velocity for each of u_e, v_e, and w_e are modeled to represent the principal eddy scales reflected in spectral data. Such data for all three velocity components

Three Models Investigated

The three different computational models investigated are distinguished mainly by their outer edge boundary conditions on velocity. The models are termed Model 1, 2, and 3 in order of increasing complexity.

Model 1.

This relatively simple model is essentially the same as that reported by Chapman and Kuhn (1981). It considers two coherent harmonic components of motion at the outer edge: one represents small scale eddies (SSE) and the other large scale eddies (LSE). The three fluctuating edge velocities are:

$$\text{Component 1} \qquad\qquad \text{Component 2}$$

$$\text{SSE} \qquad\qquad\qquad \text{LSE}$$

$$u_e = 2\alpha_1 \sin(N_1 T)\sin \zeta + [2(\alpha^2 - \alpha_1^2)] \sin(N_{u2}T + \phi_{u2})$$

$$v_e = -2\beta\sin(N_1 T)\sin \zeta \qquad\qquad\qquad\qquad\qquad (5)$$

$$w_e = 2\beta\sin(N_1 T + \phi_w)\cos \zeta + [2(\gamma^2 - \beta^2)] \sin(\frac{N_{u2}}{2} T + \phi_{w_2})$$

In order for the $(uv)_e$ correlation coefficient to be 0.45, α_1/α also must be 0.45; and hence $\alpha_1 = 0.9$. In order for $(\overline{dv^2}/dY)_e$ to be zero in accordance with experimental data, it follows that $\phi_{w1} = \pi/2$. The value $\phi_{w2} = 2\pi/3$ is determined by computer trial to yield as good agreement as possible with the law of the wall for $<U(Y)>$, the slope $(\partial<U>/\partial Y)_w = 1$ at the wall, and the Reynolds stress distribution. The value $\phi_{u2} = 0$ is also determined by computer trial to yield a reasonable level of skewness for u_e. Since N_1 is taken as .044, the computations for

The Navier-Stokes equations become*

$$\frac{\partial v}{\partial Y} + \frac{\partial w}{\partial Z} = 0$$

$$\frac{\partial u}{\partial T} + v\,\frac{\partial u}{\partial Y} + w\,\frac{\partial u}{\partial Z} = -\frac{\partial P}{\partial X} + \frac{\partial^2 u}{\partial Y^2} + \frac{\partial^2 u}{\partial Z^2}$$

$$\frac{\partial v}{\partial T} + v\,\frac{\partial v}{\partial Y} + w\,\frac{\partial u}{\partial Z} = -\frac{\partial P}{\partial Y} + \frac{\partial^2 v}{\partial Y^2} + \frac{\partial^2 v}{\partial Z^2} \qquad (4)$$

$$\frac{\partial w}{\partial T} + v\,\frac{\partial w}{\partial Y} + w\,\frac{\partial w}{\partial Z} = -\frac{\partial P}{\partial Z} + \frac{\partial^2 w}{\partial Y^2} + \frac{\partial^2 w}{\partial Z^2}$$

Thus we treat three velocity components fluctuating in two space dimensions and time (Y, Z, T). Being more than 2D flow, but not fully 3D flow, this mathematical approximation has been termed "2 ½ D" flow. An alternate descriptive term would be "slender turbulence" theory.

The boundary conditions for the differential equations at the wall are $u(0, Z, T) = v(0, Z, T) = w(0, Z, T) = 0$. At the side boundaries of the computational domain the boundary conditions are taken as periodic in each of the three velocity components. The outer edge of the computational domain is taken at $Y = 40$ for all models. The spanwise extent of this domain, however, is not the same for all models.

---

*Inasmuch as we use wall variables throughout, the + subscript will be dropped from velocity components for simplicity in the remaining sections of this text.

technique would yield $\bar{T}_{es/\lambda} \approx 120$. In the computational model $N_1 \bar{T}_{es/\lambda} = 2\pi$, so that the value above of $N_1 = .044$ corresponds to $\bar{T}_{es/\lambda} = 143$, reasonably close to the value interpreted from dye observations.

Still further elements of commonality for all models are the turbulence intensities at the outer edge of the viscous sublayer. These are inputs α, β, γ into the computations defined in wall variables as

$$\alpha = \langle u_{e+}^2 \rangle \qquad \beta = \langle v_{e+}^2 \rangle \qquad \gamma = \langle w_{e+}^2 \rangle \qquad (2)$$

The values $\alpha = 2$, $\beta = 1$, and $\gamma = 1.3$ are used throughout.

The experimental observation of highly elongate streamwise eddies in the viscous sublayer provides a basis for mathematically simplifying the models. Velocity derivatives in the streamwise X direction are neglected compared to velocity derivatives in the spanwise Z and normal Y directions. The recent turbulence simulations of Moser & Moin (1984) show that, although the u patterns are elongate streamwise, the v and w patterns are less so; hence some approximation is introduced by making this mathematical simplification.

The conventional wall variations are:

$$u_\tau^2 = \tau_w / \rho \qquad T = \frac{t u_\tau^2}{\nu} \qquad P = \frac{p}{\tau_w} = \frac{\bar{p} + \Delta p}{\tau_w}$$

$$X = \frac{x u_\tau}{\nu} \qquad Y = y_+ = \frac{y u_\tau}{\nu} \qquad Z = \frac{z u_\tau}{\nu} \qquad (3)$$

$$u_+ = \frac{u}{u_\tau} \qquad v_+ = \frac{v}{u_\tau} \qquad w_+ = \frac{w}{u_\tau}$$

$$N = \frac{n \nu}{u_\tau^2}$$

motion. The function $f(t)$ is structured such that for $o <$ $\zeta < \pi$ an ejection preceeds a sweep, whereas for $\pi < \zeta < 2\pi$ a sweep preceeds an ejection. Thus ejection/sweep and sweep/ejection events are equally numerous in the models.

The mean frequency N_1 of the SSE burst events is also taken to be the same for all models. With the Variable Interval Time Average (VITA) technique used by Blackwelder and Haritonidis (1983) to determine bursting frequency, only ejection/sweep events were counted. Since these meander spanwise over a fixed hot wire probe, their measured mean frequency of $\bar{f}_{es} \approx .0035$ would correspond to an average over space and time in the computational models. For $0 < \zeta < \pi$ the frequency of computational ejection/sweep events is $N_1/2\pi$; whereas the corresponding frequency for $\pi < \zeta < 2\pi$ is 0. Thus the average frequency of ejection/sweep events over space and time is $\bar{f}_{es} = N_1/4\pi$, which corresponds to the value

$$N_1 = 4\pi(.0035) = .044$$

This value for N_1 is not inconsistent with the mean burst period of $\bar{T}_{B/\lambda} \approx 120$ determined from visual observations with the dye technique (Schraub and Kline, 1965; Smith, 1978; Donohue et al, 1972). If an ejection preceeds a sweep, dye first accumulates along the spanwise station of the event and then becomes visible as a burst of dye when it is subsequently ejected upward. If a sweep preceeds an ejection, however, dye is first removed away from the spanwise station of the event by the sweep; and hence there may not be enough dye left at this station to make the subsequent ejection visible. Thus the "burst" frequency per λ of span from dye visualizations may represent primarily the mean frequency of ejection/sweep events, while missing most of the sweep/ejection events. If this is the case, then the dye

COMPUTATIONAL MODELS

Before describing features which distinguish between the computational models, the several features that are common to all three are to be noted. These relate to the small-scale eddy structure, and to a mathematical approximation made in view of the highly elongate streamwise eddies observed in the viscous sublayer.

Common Modeling Characteristics

In each model, the boundary condition on each velocity component is composed of two separate components structured such that the Reynolds stress at the outer edge of the viscous sublayer is produced only by a small-scale eddy component (SSE, subscript 1) that is periodic in time and space. The SSE velocity boundary conditions are of the general form

$$u_{e1} = f(t)\sin\zeta$$

$$v_{e1} = -f(t)\sin\zeta \tag{1}$$

$$w_{e1} = f(t + \phi_{w1})\cos\zeta$$

where $\zeta = 2\pi Z/\lambda$ is the dimensionless spanwise coordinate, t is time, f(t) is a periodic function with frequency N_1, and ϕ_{w1} is a phase angle to allow for the circumstance that the spanwise velocity pulse in a burst may lead (or lag) the u_{e1} and v_{e1} components. All of these quantities are in dimensionless wall variables. This SSE structure corresponds to 180° phase difference between u_{e1} and v_{e1}, in accordance with experimental observations (Wallace et al, 1977) of conditionally sampled bursting events. The spanwise variation as $\sin \zeta$ for v_{e1}, and as $\cos \zeta$ for w_{e1}, correspond to a simple contrarotating vortical

-8-

observations of Johansson, and Alfredsson (1982) have also
revealed large scale inward motions preceding an ejection
event. Their data for the smallest threshold values and the
longest integration times show that the ejection/sweep and
the sweep/ejection events are about equally numerous. Hot
wire measurements indicate that the duration of the
Reynolds-stress intensive ejection and sweep is only about
20% to 25% of the mean period between bursts. Such
observations suggest how to structure the appropriate time
phasing and duration of the two principal Reynolds-stress
producing events.

5. Coherent sublayer eddy structures are highly elongate
    streamwise. This has been observed in visual studies (Kim
    et al, 1971; Kline et al, 1967; Grass, 1971; Cantwell et al,
    1978) as well as inferred from hot wire measurements of
    spatial correlations of velocity (Blackwelder and Eckelmann,
    1979; Kreplin and Eckelman, 1979). Such observations enable
    a significant mathematical simplification to be made in the
    computational modeling.

6. There is a statistically mean period $\overline{T}_{B/\lambda}$ between
    ejection/sweep bursts per length λ of span when observed
    visually by the dye technique (Schraub and Kline, 1965;
    Smith, 1978; Donohue, et al, 1972). There is also a
    different mean period $\overline{T}$ between such bursts when measured
    by a hot wire at a fixed point in the flow. Various
    measurements of the latter show considerable scatter (e.g.
    Bandyopadhyay, 1982). Moreover, they vary with distance
    from the wall (Nakagawa and Nezu, 1981). Formerly it was
    thought that $\overline{T}$ scales on outer variables U_{∞} and δ (Laufer
    and Badri Narayanan 1971; Rao et al, 1971). However, at the
    outer edge of the viscous sublayer, where our boundary
    conditions are applied ($y_{+} = 40$), the recent measurements of
    Andreopoulos et. al. (1983) and of Blackwelder and
    Haritonidis (1983) yield the relatively consistent result of
    $\overline{T}_{+} \simeq 250$ to 300.   This result is essentially independent of
    Reynolds number over the range $10^3 < Re_{\theta} < 1.5 \times 10^4$
    covered by these two sets of experiments; and is used to set
    the value of $\overline{T}_{B/\lambda}$ for numerical computations.

7. The principal Reynolds-stress production is intermittent,
    consisting of periods of relative quiescence terminated by
    burst events. This has been reported from visual studies
    (Corino and Brodkey, 1969; Offen and Kline, 1975; Praturi
    and Brodkey, 1978; Nychas et al, 1973) and from hot wire
    measurements (Blackwelder and Kaplan, 1976). Recent

3. Streamwise streaks of low-speed and high-speed fluid
    alternate spanwise. This streaky structure has been
    observed visually near a wall in both the velocity pattern
    (Kline et al, 1967) and the temperature pattern (Hirata et.
    al. 1982; Iritani et. al. 1983). It has also been detected
    in hot wire measurements (Gupta et al, 1971), and in large
    eddy numerical simulations of turbulence (Moin and Kim,
    1982). Many experiments have demonstrated that the mean
    spanwise spacing between low-speed streaks is $\lambda_+ \simeq 100$ for
    the R_e range of usual laboratory experiment. Schraub and
    Kline (1965) found the value of λ_+ to be insensitive to
    pressure gradient. Offen and Kline (1975) suggest that
    successive streamwise generations of low-speed streaks
    appear to be staggered spanwise in a checkerboard like
    fashion. Such observations provide a guide for structuring
    the spanwise distribution of the streamwise velocity.

4. Streamwise vortical motions are the dominant Reynolds-stress
    producing eddy structure in the VSL. Visual observations
    have revealed stretched streamwise vortical motions (Kim et
    al, 1971; Kline et al, 1967; Clark and Markland, 1969) as
    well as contrarotating pairs (Smith, 1978). Presence of
    vortex pairs has also been inferred from various correlation
    data (Bakewell and Lumley, 1967; Lee et al, 1974; Willmarth,
    1975; Blackwelder and Eckelmann, 1979; Kreplin and
    Eckelmann, 1979). Recently, the conditional averaging
    technique has been applied to numerically computed turbulent
    flow in a channel (Kim 1983, 1984), and has revealed clearly
    that a pair of counter rotating streamwise structures
    accompanies ejection and sweep events. Thus, the principal
    Reynolds-stress producing events are associated with
    vortical pairs, although single streamwise vortical
    structures appear more common than pairs (Moser and Moin,
    1984). These various observations provide a guide for
    structuring the spanwise variations of the normal and
    spanwise components of velocity.

NUMERICAL COMPUTATION METHOD

A computer code recently developed by Kim and Moin (1984) was adapted to the conditions of this study. The reader is referred to their report for details of the numerical algorithms. A brief qualitative description is given herein of the numerical method along with an account of the modifications made for the present computations.

With the pressure gradient split into three terms, the Navier-Stokes equations in tensor notation are

$$\frac{\partial U_i}{\partial T} - \frac{\partial}{\partial x_j}(U_i U_j) - \frac{\partial P}{\partial x_i} - \frac{\partial \overline{P}}{\partial x_i} + F_i(T) + \nabla^2 U_i \qquad (15)$$

$$\frac{\partial U_i}{\partial x_i} = 0 \quad i = 1,2,3 \qquad (16)$$

where U_i = the velocity components U,V,W corresponding to $i = 1,2,3$, respectively

$\overline{P}$ = the mean pressure normalized by the wall shear stress, τ_w

P = the pressure perturbation normalized by the wall shear stress

F_i = a body force used in Model 1 which corresponds to a global pressure gradient associated with the LSE

x_i = the Cartesian coordinates X,Y,Z in wall variables

The equations are to be solved in a rectangular region $0 < Y < Y_e$, $0 < Z < ZMAX$. The flow is assumed to be periodic in Z with zero velocity at $Y = 0$. At $Y = Y_e$, the boundary conditions are

$$U_i(X, Y_e, Z) = U_{i_{e1}}(Z, T) + U_{i_{e2}}(T) \qquad (17)$$

In model 1, the functions $F_i(T)$ are taken to correspond to the LSE pressure gradients of simple oscillating shear flow in the X and Z directions. Thus, for this model

$$F_i(T) = \frac{\partial U_{1_{e2}}}{\partial T} = \frac{\partial u_{e2}}{\partial T} \qquad (18)$$

$$F_2(T) = 0 \qquad (19)$$

$$F_3(T) = \frac{\partial U_{3_{e2}}}{\partial T} = \frac{\partial w_{e2}}{\partial T} \qquad (20)$$

and the mean pressure, $\overline{P}$, is assumed to be a function of X alone. For models 2 and 3, $F_i(T)$ was set to zero.

For numerical solution of Eqs. (15) and (16), Kim and Moin use an Adams-Bashforth formula for convective terms, and centered differences for viscous terms. A factored semi-implicit solution algorithm is used that is explicit in convective terms, and implicit in viscous terms. The first step in time-advancing the solution calculates a predictor velocity field which satisfies appropriate boundary conditions, but not the continuity equation. A second step then corrects the velocity field to satisfy the continuity equation and the Poisson equation for pressure. The method is second-order accurate in both space and time.

An accuracy test of the Kim-Moin code was made by computing oscillating shear flow and comparing results with exact analytical solutions (Chapman and Kuhn, 1981). With 320 time steps per cycle, and 17 points uniformly spaced across the oscillating layer, the numerical method was found to be very accurate (indistinguishable from the exact analytical solution on a normal size plot).

In making numerical computations, an arbitrary initial
velocity profile is needed at $T = 0$. To accelerate convergence
to periodicity, an analytical approximation for a turbulent
boundary layer profile was used. The boundary conditions at Y_e
were multiplied by an exponential factor which starts at zero and
reaches unity asymptotically over the first time cycle of the
computation. The solution was then advanced until periodic flow
conditions were attained, usually after about 3 or 4 cycles of
time for Models 1 and 2. Space and time averages were then taken
over a cycle of periodic flow. A typical computation of viscous
sublayer turbulence for our normal mesh used 400 time steps per
small-scale cycle, 30 points in the Y direction; 32 points in the
Z direction; and, for models 1 and 2, required 4 to 5 minutes of
CRAY X-MP time per run. The corresponding run time for model 3
was considerably longer due to the lack of periodicity. For the
special fine mesh used to define the near-wall behaviour of
turbulence, up to 3200 time steps per small-scale cycle were used
with 60 points in the Y direction, 64 in the Z direction, and a
run time of over one hour.

The computational method was found to be quite stable as
long as the time step was smaller than a certain value which
depends on the spatial grid size. The particular value was
determined by trial and error for each grid. Below the
instability limit, the solution obtained was not strongly
dependent upon the time step size, but was affected somewhat by
the spatial grid.

Calculation of statistical quantities

The computation of the time dependent dynamics of the flow
was followed by time and spanwise space averaging of the
results. This produces profiles of statistical characteristics
of the flow field which can then be compared with measured

data. For models 1 and 2, the quantities of interest were computed by calculating three time-cycles of the periodic solution after convergence to periodicity was attained. Three cycles were used in order to allow the computation of the appropriate mean values from which various perturbations are calculated. The quantities calculated in each cycle were as follows, wherein < > designates the time and spanwise space average:

First Cycle: Calculate $\langle u \rangle$, $\langle v \rangle$, and $\langle w \rangle$

Second Cycle: Re-calculate $\langle u \rangle$, $\langle v \rangle$, and $\langle w \rangle$, then $u - \langle u \rangle$, $v - \langle v \rangle$, and $w - \langle w \rangle$, then calculate $\langle u - \langle u \rangle \rangle$, $\langle v - \langle v \rangle \rangle$, and $\langle w - \langle w \rangle \rangle$, and all cross-products, such as $\langle (u - \langle u \rangle)(v - \langle v \rangle) \rangle$, etc. Also calculate the higher order products, such as $\langle (u - \langle u \rangle)^2 \rangle$, $\langle (u - \langle u \rangle)^3 \rangle$, and $\langle (u - \langle u \rangle)^4 \rangle$, and the derivatives and products needed to calculate the dissipation.

Third Cycle: Calculate the perturbations from the mean Reynolds Stress and the various products needed to calculate the intensity of $\langle uv \rangle$ fluctuations, and the Skewness and Flatness of $\langle uv \rangle$ fluctuations. It is noted here that all products were computed. That is, the results were not limited to products of the u and v components, but also include the w component. However, most data comparisons are made with the u and v components, and the combinations of those components that make up the Reynolds stress and various perturbation statistics of the Reynolds stress.

For Model 3, a slightly revised procedure was followed. Since there is no periodicity in the time variation of the solution, all calculated values must be included in the statistical summations. In order to minimize the computer time and storage requirements, the formulas for the most interesting statistical quantities were derived, to allow the calculation to

be done in a single pass, and to allow the calculation to be done in stages. In this way new results could be calculated as a continuation of previous results. The quantities so determined are as follows:

Mean Value

$$\langle u \rangle = \frac{1}{N_z N_t} \sum_1^{N_z} \sum_1^{N_t} u_{ij} \tag{21}$$

Turbulence Intensity

$$u'^2 = \langle (u - \langle u \rangle)^2 \rangle = \langle u^2 \rangle - \langle u \rangle^2 \tag{22}$$

Cross Correlations (e.g. Reynolds stress)

$$\langle (u - \langle u \rangle)(v - \langle v \rangle) \rangle = \langle uv \rangle - \langle u \rangle \langle v \rangle \tag{23}$$

Intensity of Reynolds Stress Fluctuations

$$\langle [(u - \langle u \rangle)(v - \langle v \rangle) - \langle uv \rangle]^2 \rangle \tag{24}$$

$$= \langle u^2 v^2 \rangle + \langle u \rangle^2 \langle v^2 \rangle - 2\langle uv^2 \rangle \langle u \rangle - \langle uv \rangle^2$$

Skewness of Velocity Fluctutations

$$S = \frac{\langle u^3 \rangle + 2 \langle u \rangle^3 - 3 \langle u \rangle \langle u^2 \rangle}{[\langle u^2 \rangle - \langle u \rangle^2]^{3/2}} \tag{25}$$

Flatness of Velocity Fluctuations

$$F = \frac{\langle u^4 \rangle - 4\langle u^3 \rangle \langle u \rangle + 6\langle u^2 \rangle \langle u \rangle^2 - 3\langle u \rangle^4}{[\langle u^2 \rangle - \langle u \rangle^2]^2} \tag{26}$$

Each of these quantities contains terms which are functions of y only and are obtained from sums of the quantities at each point. Thus, calculations can be carried out to any number of

steps by storing the value of the sums at each step, allowing the calculation of a few steps at a time until examination of the results indicates a statistical steady state has been achieved. This results in a greatly reduced storage requirement and computer cost compared to the approach used for periodic solutions which would require storing the entire flow field array at each time step in order to compute the complete statistics.

Generation of Random Numbers

In generating a sequence R_n of N random numbers, a new parameter C is introduced representing the correlation coefficient between successive terms R_n and R_{n-1} of the sequence. That is,

$$C = \overline{R_n R_{n-1}} \tag{27}$$

where $\overline{R_n R_{n-1}}$ is the average value of the product over all terms over a long time period of the sequence. The sequence is constructed to have an rms variance of unity. The relationship between a sequence of random numbers R_n^* generated by a computer and the desired random function with correlation C is relatively simple. If the sequence R_n^* has a mean value of $\overline{R_n^*}$ and an rms value of σ, the corresponding random function with unit rms is (Moshman, 1967)

$$R_n = C R_{n-1} + [\sigma^2 (1-C^2)] (R_n^* - \overline{R_n^*}) \tag{28}$$

Thus, a sequence with mean value of zero and rms value of 1 can be generated from any random sequence.

A measure of the time scale of the sequence R_n is found by calculating the integral of the autocorrelation of the sequence. Thus,

$$I_t = \Delta T \int_0^\infty \int_0^\infty R_n R_{n+m} \, dmdn \tag{29}$$

This integral time scale in wall variables can be used to determine a value for the correlation coefficient C since the autocorrelation for the sequence (R_n) is C^n, and therefore,

$$I_t = \Delta T \int_o^\infty C^n \, dn = \frac{\Delta T}{\ln(1/C)} \qquad (30)$$

where ΔT represents the time step between successive terms. Thus,

$$C = e^{-\Delta T/I_t} \qquad (31)$$

Since the integral time scale of turbulence for a given velocity component depends upon Reynolds number, the correlation coefficient will be a function of both Reynolds number and the time step taken in the numerical computations.

Data on the integral time scale of turbulence near the outer edge of the viscous sublayer (Y = 40 to 50) have been obtained from the experiments of Comte-Bellot (1963), Fulachier (1972), Elena (1977), and Hofbauer (1978). Their data are shown in figure 3 as a function of δ_+, the boundary layer (or half channel) thickness expressed in wall units. The integral time scale was determined from experimental measurements of autocorrelation for each velocity component. Each set of experimental data was taken at a different δ_+, and hence different Reynolds number. These data, together with the Reynolds number and time step used in numerical calculation, determine the appropriate correlation coefficient to be used for each velocity component in generating the random time functions R_{u2}, R_{v3} R_{w3}.

A typical time step used in the numerical calculations is

$$\Delta T = \frac{2\pi}{N \, N_1} \qquad (32)$$

where N is the total number of steps used in the numerical calculation of one cycle of the small-scale, and N_1 is the frequency, defined previously. At the location Y = 40, the data of figure 3 indicate that the integral time scales of the v and w components are approximately equal at 8 wall units of time while that of the u component is approximately 42 wall units. The corresponding values of the correlation coefficient are obtained from

$$C = e^{-\frac{2\pi}{N\,N_1\,I_t}} \qquad (33)$$

which yields values of C from 0.95 to 0.99 for the values of N and N_1 typically used in the numerical calculations. In order to provide an illustrative calculation and keep computer time within acceptable bounds, the value of C = 0.95 was used in the numerical computations for Model 3.

In order to obtain meaningful results for the statistical quantities, the random sequences must be calculated until a steady state is reached. The number of steps required for this is not known a priori. Due to the combination of periodic and random functions, the total number of steps used must be an integral number of periods of the small scale components. For the results discussed herein, the calculations were carried out until two successive cycles resulted in a negligible change of the accumulated statistics.

COMPUTATIONAL RESULTS COMPARED
WITH EXPERIMENT

Law of the Wall - As illustrated in figure 4, the mean
streamwise velocity profile computed for models 1 and 2 agree
well with experiment. For model 3, however, the computed values
of <U> are a little low. Because of the relatively long
computer times required when random time functions are used,
systematic variations in the parameters of model 3 were not
explored. It is possible, therefore, that modest changes in
these parameters could bring the computed <U> profiles for model
3 into agreement with experiment comparable to that of model 1
and 2.

Intensity of Turbulence - The computed rms intensity of
streamwise turbulence u' is not greatly different for the three
models (figure 5a). Each model yields peak values of u' higher
than experiment. For models 2 and 3, some irregularities can be
seen near the outer edge of the viscous sublayer (Y between about
35 and 40). This irregularity, as shown later, is manifested in
a more pronounced outer-edge anomaly in the rate of dissipation
and the intensity of streamwise vorticity fluctuations. The
slope of the curve of u'(Y) at Y = 0 is equal to
$S_x' = <(\tau_{xw} - <\tau_{xw}>)^2>^{1/2}/<\tau_w>$ the fluctuating intensity of
streamwise wall shear stress. In wall units, computed values of
S_x' for the normal mesh are 0.55, 0.47 and 0.50 for models 1, 2,
and 3, respectively. These values are higher than experimental
values which range between 0.24 and 0.49. Runs with finer mesh
intervals did not change appreciably the computed values of S_x'.

The computed intensity of turbulence v' normal to the wall
is nearly the same for all three computational models (figure
5b). Although the experiments indicate higher values of v' near
the wall, this may be due in sizeable part to experimental

-27-

errors, since hot-wire measurements of v' are notoriously
inaccurate near a wall. Most of the experimental data, in fact,
extrapolate erroneously to non-zero values at the wall.

The computational curves of spanwise turbulence intensity w'
(figure 5c) show more variation between the three models.
Although the computed levels of w' are in reasonably good
agreement with experiment for all three models, some irregularity
is exhibited near the outer edge. At the wall, the slopes of the
w' curves, representing the intensity of spanwise shear stress
fluctuations, are 0.14 and 0.31 for Models 1 and 2,
respectively. These values were determined from runs with a fine
mesh. Expermental values are about 0.1.

Reynolds Stress - The computed distributions of <uv> as
might be expected, show similar results to those for
<U(Y)>. This is illustrated in figure 6a. For models 1 and 2
the Reynolds stress computations agree very well with experiment,
but for model 3 the computed values are somewhat low. In the
case of model 1 the parameters ϕ_{w2} and ϕ_{u2} were determined by
computer trial to provide good agreement with Reynolds Stress
measurements; and in the case of model 2, the parameters
ϕ_{w3} and ϕ_{u2} were determined likewise; but, for model 3 these
parameters do not appear. The parameters β_1 and γ_1, however,
were found in models 1 and 2 to affect <uv> significantly, and
presumably could be adjusted in Model 3 to provide better
agreement with experiment for both <uv> and <U(y)>. Primarily
because of the long computer times required for model 3, however,
such parameter adjustments were not investigated.

The computed rms fluctuations in Reynolds Stress as shown in
figure 6b also differ relatively little between the three
models. Considering that the experimental data scatter widely -
because of the inherent difficulty of such measurements very near
a wall - the agreement between computation and experiment is
reasonably good.

It is to be noted that in the outer region of the viscous sublayer, the rms fluctuations in uv are about twice the mean value $\overline{uv}$, for both computation and experiment.

Skewness and Flatness Factor - Distributions of skewness and flatness factor for the streamwise velocity fluctuations are presented in figure 7. Near the wall, both skewness and flatness are low for Model 1 with its simple harmonic boundary conditions on velocity. For model 2, which simulates more realistically the intermittent character of burst events, these factors are in much better agreement with experiment near the wall, as might be expected. In the case of model 3 with randomly generated time functions, the skewness and flatness of u' are considerably greater than for model 2 and the experimental data. The reason for this is uncertain. A possible cause may be that these higher order statistics may require larger computation times to reach steady conditions than do the lower order statistics such as u', v', etc.

Similar characteristics are exhibted by the skewness and flatness factor for the fluctuating Reynolds stress (figure 8a and 8b). Here again, the flatness factor for model 2, agrees better with experiment than does model 1. Computations were not made of the Reynolds Stress skewness and flatness for model 3.

Correlation Coefficient R_{uv} As shown in figure 9, all three models yield values of R_{uv} between about 0.4 and 0.5 in the outer three-fourths of the viscous sublayer. The computations for models 3 and 2 exhibit very similar trends, indicating that the use of random time functions in place of periodic ones has only a small effect on the u-v correlation. Experimental data scatter widely below about Y of 10, with one data set (Eckelmann 1974) suggesting increasing values of R_{uv} as the wall is approached, whereas another set (Kutateladze 1977) indicates strongly

decreasing values. Considering the wide scatter of these experimental data, all three models yield acceptable computations of R_{uv}.

Dissipation and Streamwise Vorticity Fluctuation - These two quantities illustrated in figure 10 reveal most clearly the existence of an anomaly in all three models near the outer edge of the viscous sublayer. Both the rate of turbulence dissipation ϵ, and the rms intensity of fluctuating streamwise vorticity Ω'_x, exhibit anomaloulsy high values in the outer region between about Y = 35 and Y = 40. Since ϵ and Ω'_x reflect the magnitude of velocity gradients, it is clear that all three models produce a region near the outer edge in which velocity gradients are large and vary rapidly with Y. Such a region is of the "Stokes-Layer" type. It is believed due to some unrealistic or artificial aspect of the velocity boundary conditions imposed at Y = 40, to which the Navier-Stokes equations make rapid adjustment, leaving most of the turbulence characteristics below Y of about 35 in reasonable accord with reality.

Inasmuch as dissipation rate is a quantity often used in Reynolds-average modeling to determine the important length scale of turbulence, an effort was undertaken to vary the model parameters and eliminate, if possible, this undesirable anomaly. Systematic variations were made in the parameters α_1, β_1, γ_1, N_1, N_{u2}, N_{v3}, N_{w3}, ϕ_{w1}, ϕ_{u2}, ϕ_{w2}, ϕ_{w3}, λ, X,M, and $(Y)_e$. While some of these variations altered somewhat the high value of ϵ at the outer edge, none eliminated or reduced it by more than a factor of about 2. In addition, phase angles in spanwise space and in time for the intermediate-scale component of model 2 were introduced and varied; but without any essential effect on the anomaly. Moreover, the spanwise profiles of velocity were altered from $\sin \zeta$ to $\sin^p \zeta$, with p being a power greater or less than one, and still the anomaly remained. When runs were

made with only the small-scale eddy components present, and without any large or intermediate scale components, it was found that the anomaly still existed. On the other hand, it was not present when only the large-scale components of velocity were used. We conclude, therefore, that the outer-edge anomaly is a consequence of some unrealistic aspect in the structure of the velocity boundary conditions for the small-scale eddies which produce the Reynolds Stress in all three models.

It may be noted that the Stokes-layer anomaly at the outer edge is not attributed to the approximation of 2.5D flow. In principle, the velocity fields computed at Y of 30, say, could have been used as outer-edge boundary conditions imposed at $Y_e = 30$, and identical results would have been produced below Y of 30 without an anomaly. A cursory examination of the velocity fields at Y = 30, however, showed them to be rather complex. More detailed study of such fields, however, might provide a guide as to how the small-scale eddy velocity components could properly be constructed without producing an anomaly at the outer edge.

NEAR-WALL LIMITING BEHAVIOUR OF TURBULENCE

Experimental techniques have not been able to determine the limiting behaviour of turbulence very near a wall. As a consequence, several different ideas have been advocated. Over thirty years ago, Reichardt (1951) concluded that for streamwise inhomogeneous flows, u' would be proportional to y, v' to y^2, and $\overline{uv}$ to y^3, as y approaches zero; but that for streamwise homogeneous flows $\overline{uv}$ would be proportional to y^4. Elrod (1957) arrived at the same conclusion. The widely used and highly successful damping-factor model of Van Driest (1956) corresponds also to $\overline{uv} \sim y^4$. . Some support for this appeared to be provided by the theoretical results of Ohji (1967) for homogeneous flows which also yield near the wall

$\overline{uv} \sim y^4$, together with $R_{uv} \sim y$, and $(R_{uv})_w = 0$. A review of the differing views on the y^3 versus y^4 controversy has been given by Hinze (1975).

Numerical computations from the Navier-Stokes equations offer a means of resolving this issue. Towards this end computations with very fine meshes and small Courant numbers have been made for models 1 and 2 for the case of zero pressure gradient. (Considerations of computer time precluded doing this for model 3.) In the y direction 60 points were used across the viscous sublayer, with clustering near the wall and with the closest point at $Y = .018$. In the z direction 64 points were used evenly spaced spanwise. Due presumably to a numerical truncation error at the wall boundary, the wall turbulence values were not precisely zero (ranging from 10^{-12} for <uv> to 10^{-4} for w') and were subtracted out in order for the turbulence to be precisely zero at the wall. The results are shown as log-log plots in figures 11 and 12 for the range of Y between .01 and 10. The limiting near-wall behavior in each model is clearly $u' \sim y$, $v' \sim y^2$, $w' \sim y$, <uv> $\sim y^3$, and $(R_{uv})_w = $ constant $\neq 0$. The constants of proportionality, of course, differ between the two models: R_{uv} near the wall, for example, approaches 0.34 for model 1, and 0.21 for model 2. But the limiting power law exponents are precisely the same for the two models. It is noteworthy that the range of validity of the limiting power laws is quite different for different turbulence quantities: $u' \sim y$ out to Y of about 3 or 4, while $v' \sim y^2$ and $R_{uv} = $ constant out to Y of only about 0.3.

In general, the near-wall limiting behavior extends to Y of about 0.3. Between $0.3 < Y < 3$, R_{uv}, v', and w', especially for model 2, depart considerably from their respective limiting near-wall power laws.

References (cont.)

Hatziavramidis, D. T. and Hanratty, T. J., (1979): The
Representation of the Viscous Wall Region by a Regular Eddy
Pattern. J. Fluid Mech., Vol. 95, Pt. 4, p. 655.

Hinze, J. O. (1975): Turbulence, McGraw-Hill 2nd Ed. p. 621.

Hirata, M., Tanaka, H., Kawamura, H. and Kasagi, N. (1982):
Heat Transfer in Turbulent Flows, Proc. Seventh International
Heat Transfer Conference, Munchen, Sept. 6-10 1982, Vol. 1,
pp. 31-57.

Hofbauer, M. (1978): Visuelle und Anemometrische
Untersuchung Koharenter Structuren im Geschwindigkeitsfeld
einer Ausgebildenten Turbulenten Kana stromung. Max-Plank-
Institute Fur Stromungsforschung, Gottingen, Report 66.

Hogenes, J. H. A. and Hanratty, T. J., (1982): The use of
Multiple Wall Probes to Identify Coherent Flow Patterns in
the Viscous Wall Region, J. Fluid Mech., Vol. 124, pp. 363-

Hussain, A. K. M. F. and Reynolds, W. C., (1975):
Measurements in Fully Developed Turbulent Channel Flow. J.
Fluids Engrg., Vol. 97, pp. 568-578.

Iritani, Y., Kasagi, N., and Hirata, M. (1983): Heat
Transfer Mechanism and Associated Turbulence Structure in the
Near-Wall Region of a Turbulent Boundary Layer. Proc. 4th
Symposium on Turbulent Shear Flows.

Johansson, A. V. and Alfredsson, P. H. (1982): On the
Structure of Turbulent Channel Flow. Jour. Fluid Mech., Vol.
122, pp. 295-314.

Kaneda, Y. and Leslie, D. C. (1982): Tests of Subgrid Models
in the Near-Wall Region Using Represented Velocity Fields. J.
Fluid Mech, Vol. 132, pp. 349-373.

Kasagi, N., Hirata, M. and Nishino, K. (1984): Streamwise
Pseudo-Vortical Structures and Associated Vorticity in the
Near-Wall Region of a Wall-Bounded Turbulent Shear Flow,
Paper presented at 9th Biennial Symposium on Turbulence,
Univ. of Missouri-Rolla, Rolla, Missouri.

Kastrinakas, E. G., and Eckelmann, H. (1983): Measurement of
Streamwise Vorticity Fluctuations in a Turbulent Channel
Flow, J. Fluid Mech., Vol. 137, pp. 165-

Kastrinakas, L., Wallace, J. M., and Willmarth, W. W.
(1975): Measurements of Small Scale Streamwise Vorticity in
a Turbulent Channel Flow. Bull. Amer. Phys. Soc. Vol. 20, p.
1422.

References (cont.)

Comte-Bellot, G. (1963): Turbulent Flow Between Two Parallel Walls. Thesis, Univ. of Grenoble. Translation A.R.C. 31609, F.M. 4102.

Donohue, G. L, Tiederman, W. G., and Reischman, M. M., (1972): Flow Visualization of the Near-Wall Region in a Drag-Reducing Channel Flow. J. Fluid Mech., Vol. 56, Pt. 3, pp. 559-575.

Eckelmann, H., (1974): The Structure of the Viscous Sublayer and the Adjacent Wall Region in a Turbulent Channel Flow. J. Fluid Mech., Vol. 65, Pt. 3, pp. 439-459.

Elena, (1977): Etude Experimentale de la Turbulence on Voisinage de la Paroi d'un Tube Legerment Chauff. Int. Jour. Heat & Mass Transfer, 20, pp. 935-944.

Elena, M., Fulachier, D., and Dumas, R., (1979): Etude Experimentale des Apports et des Ejections de Fluid Dans une Couche Limite Turbulent. AGARD CPP271, pp. 2-1 2-21.

Elrod, H. G. (1957): Note on the Turbulent Shear Stress Near a Wall, Jour. Aero. Sci. 24, pp. 468-469.

Entoma, R. A., Rajagopalan, E., Subramanian, C. S., and Chambers, A. J. (1982): Reynolds Number Reference of the Structure of a Turbulent Boundary Layer, J. Fluid Mech., Vol. 121, pp. 123-140.

Falco, R. E., (1977): Coherent Motions in the Outer Region of Turbulent Boundary Layers. Phys. Fluids, Vol. 20, No. 10, Pt. II, pp. S124-S132.

Fulachier, L. (1972): Contribution a L'Etude des Analogies des Champs Dynamique et Thermique dans une Couche Limite Turbulent. Effect de l'Aspiration, Thesis, University of Provence, France.

Grass, A. J., (1971): Structural Features of Turbulent Flow Over Smooth and Rough Surfaces. J. Fluid Mech., Vol 50, Pt. 2, pp. 233-255.

Gupta, A. K. and Kaplan, R. E., (1972): Statistical Characteristics of Reynolds Stress in a Turbulent Boundary Layer. Phys. Fluids, Vol. 15, No. 6, pp. 981-985.

Gupta, A. K., Laufer, J., and Kaplan, R. E., (1971): Spatial Structure in the Viscous Sublayer. J. Fluid Mech., Vol. 50, Pt. 3, pp. 493-512.

REFERENCES

Andreopoulos, J., Durst, F., and Jovanovic, J. (1983): On
the Structure of Turbulent Boundary Layers at Different
Reynolds Numbers, 9th Symposium on Turbulent Shear Flows, pp.
2.1 - 2.5.

Badri Narayanan, M. A. and Marvin, J. G., (1978): On the
Period of the Coherent Structure in Boundary Layers at Large
Reynolds Numbers. NASA TM 78477.

Bakewell, H. P. and Lumley, J. L., (1967): Viscous Sublayer
and Adjacent Wall Region in Turbulent Pipe Flow. Phys.
Fluids, Vol. 10, No. 9, pp. 1880-1889.

Bandyopadhyay, P. R. (1982): Period Between Bursting in
Turbulent Boundary Layers. Phys. Fluids, Vol. 25 (10), pp.
1751-1754.

Blackwelder, R. F. and Eckelmann, H., (1979): Streamwise
Vortices Associated with the Bursting Phenomenon. J. Fluid
Mech., Vol. 94, Pt. 3, pp. 577-594.

Blackwelder, R. F. and Haritonidis, J. H.,(1983): Reynolds
Number Dependence of the Bursting Frequency in Turbulent
Boundary Layers. J. Fluid Mech., Vol. 132, pp. 87-103.

Blackwelder, R. F. and Kaplan, R. E.,(1976): On the Wall
Structure of the Turbulent Boundary Layer. J. Fluid Mech.,
Vol. 76, Pt. 1, pp. 89-112.

Brown, G. L. and Thomas, A. S. W., (1977): Large Structure
in a Turbulent Boundary Layer. Phys. FLuids, Vol. 20, No.
10, Pt. II, pp. S243-S252.

Cantwell, B., Coles, D., and Dimotakis, P., (1978):
Structure and Entrainment in the Plane of Symmetry of a
Turbulent Spot. J. Fluid Mech., Vol. 87, Pt. 4, pp. 641-672.

Chen, C. H. and Blackwelder, R. (1978): Large-Scale Motion
in a Turbulent Boundary Layer: A Study Using Temperature
Contamination. Jour. Fluid Mech., Vol. 89, Pt. 1, pp. 1-31.

Clark, J. A., (1968): A Study of Turbulent Boundary Layers
in Channel Flow. J. Basic Engrg., Vol. 90, pp. 455-465.

Clark, J. A. and Markland, E., (1969): Vortex Structures in
Turbulent Boundary Layers. Aero Jour. Roy. Aero. Soc., Vol.
74, pp. 243-244.

Corino, E. R. and Brodkey, R. S., (1967): A Visual
Investigation of the Wall Region in Turbulent Flow. J. Fluid
Mech., Vol. 37, Pt. 1, pp. 1-30.

ACKNOWLEDGEMENTS

No variation, y^0 R_{uv}, $u'/\langle U \rangle$, $w'/\langle U \rangle$, $2\overline{k}-\epsilon$, $\overline{k}-y(\partial\overline{k}/\partial y)$

y variation u', $v'/\langle U \rangle$, w', $(\Omega_x' - \Omega_{xw}')$, Ω_y', $(\Omega_z' - \Omega_{zw}')$, $(\epsilon-\epsilon_w)$

y^2 variation v'

y^3 variation $\langle uv \rangle$

positive correlation between u and ∂w/∂z, and this requires a y^3 variation to conserve mass. Since these fundamental coherent motions have been observed in flows with streamwise pressure gradient as well as without, in streamwise homogeneous as well as inhomogeneous flows and over curved as well as flat surfaces, the y^3 variation is concluded to be rather general. The constant of proportionality, of course, may depend upon pressure gradient and curvature.

It is noted that the limiting power laws for several of the turbulence quantities, are accurate only for Y less than about 0.3. This is a surprisingly small domain. In the range 0.3 < Y < 3, power laws are still a good approximation, but the exponents change a little: to less than one for w', less than 2 for v', and to slightly greater than 3 for $\overline{uv}$. The u-v correlation varies considerably over this range.

The several applications made to Reynolds-average turbulence modeling are illustrative of the way in which time-dependent Navier-Stokes computations can be used to strengthen practical methods of turbulence computation. A number of uncertain elements still exist in the important ε- transport equation which is commonly used to determine the length scale of turbulence. They could be resolved with improved computational models that are more accurate for dissipation than the present models.

The observed limiting behavior of various turbulence quantities near a wall, as reflected in the exponent of their limiting power-law behavior, is summarized as follows:

CONCLUDING REMARKS

Three different computational models for incompressible viscous sublayer turbulence have been investigated. They are characterized by different velocity boundary conditions imposed on the time-dependent Navier-Stokes equations at the outer edge of the viscous sublayer. Although these boundary conditions differ significantly, they yield surprisingly similar results for most of the turbulence quantities. All models, for example, yield reasonably realistic computations of mean streamwise velocity, Reynolds stress, u-v correlation coefficient, and of the fluctuating intensities of velocity and Reynolds Stress. Relative to model 1, which is the simplest, the principal merit of model 2 is that it yields more realistic values for the skewness and flatness factors near the wall. Model 3, which requires much more computation time than either model 1 or 2, does not appear to yield significant improvement over model 2, and relatively little over model 1.

All three models exhibit near the outer edge of the viscous sublayer a thin region in which velocity gradients vary rapidly from anomalously high values at the outer edge (Y = 40) to reasonably realistic values at Y values of about 30 to 35. In this thin, Stokes-layer region, both the rate of turbulent energy dissipation and the rms fluctuations in streamwise vorticity are anomalously high. This is the principal shortcoming of the models. The outer-edge anomaly is attributed to some unrealistic aspect about the small-scale eddy structure in the boundary conditions.

The limiting third-power variation of Reynolds stress near a wall is concluded to be very general because of the physical explanation underlying it. In essence, organized sweep and ejection motions that produce Reynolds stress also produce

$$\epsilon_w = \bar{k} - y \; \partial \bar{k}/\partial y$$

$$\frac{\partial \epsilon}{\partial y} = \left(\frac{\partial \epsilon}{\partial y}\right)_w = 2 \; \frac{\partial \bar{k}}{\partial y}$$

$$\epsilon_w = 2k - \epsilon$$

As illustrated in figure 15, the quantity $\left(\bar{k} - y \frac{\partial \bar{k}}{\partial y}\right)_+$ is very nearly constant near the wall. It is equal to the wall dissipation $\left(\epsilon_+\right)_w$ within 0.1 percent up to about $Y = 0.6$, and within 1 percent up to about $Y = 1.3$. The quantity $\partial \epsilon/\partial y$ is nearly constant up to about $Y = 0.3$. The quantity $2\bar{k} - \epsilon$ in the numerical computations is equal to the wall dissipation within 1 percent out to about $Y = 0.8$. For some numerical algorithms, a boundary condition involving only a first derivative, or no derivative, is preferable to one involving a second derivative. The fourth equation listed above probably provides the simplest wall boundary condition for use in the ϵ transport equation.

$$u = a_1 y + a_2 y^2 + 0 \ (y^3)$$

$$w = b_1 y + b_2 y^2 + 0 \ (y^3)$$

$$v = \quad c_2 y^2 + 0 \ (y^3)$$

where the coefficients a_1, a_2, b_1, b_2, and c_2 are functions of x, z, and t. Hence,

$2k/y^2 = (\overline{a_1^2} + \overline{b_1^2}) + 2(\overline{a_1 a_2} + \overline{b_1 b_2})y + 0(y^2)$. Disregarding the very small contribution of spanwise derivatives to ε, we have

$$\varepsilon = \overline{\left(\frac{\partial u}{\partial y}\right)^2} + \overline{\left(\frac{\partial w}{\partial y}\right)^2} + \overline{\left(\frac{\partial v}{\partial y}\right)^2} = \overline{(a_1 + 2a_2 y)^2} + \overline{(b_1 + 2b_2 y)^2} + 0(y)^2$$

$$= (\overline{a_1^2} + \overline{b_1^2}) + 4 \ (\overline{a_1 a_2} + \overline{b_1 b_2})y + 0(y^2)$$

from which it follows that $\varepsilon_w = \partial^2 k / \partial y^2 = (\overline{a_1^{\ 2}} + \overline{b_1^{\ 2}})$, and that near the wall $(\varepsilon - \varepsilon_w)$ varies linearly with y. It also readily follows from manipulation of the above equations that the rms streamwise and spanwise vorticity vary similarly, e.g., $(\Omega_x' - \Omega_{xw}') \sim y$ and $(\Omega_z' - \Omega_{zw}') \sim y$; but that the rms normal vorticity $\Omega_y' \sim y$ since $\Omega_{yw}' = 0$.

With $C \equiv (\overline{a_1 a_2} + \overline{b_1 b_2})$, and $\overline{k} \equiv 2k/y^2$, it follows that the first two terms in the near-wall expansion are

$$\varepsilon = \varepsilon_w + 4 \ Cy$$

$$\frac{2k}{y^2} \equiv \overline{k} = \varepsilon_w + 2 \ Cy$$

Since $\partial \overline{k} / \partial y = 2C$, four alternate near-wall limiting equations for dissipation follow from these two equations. These four equations are valid within the small but finite Y range of limiting near-wall behavior.

$$\varepsilon_w = \partial^2 k / \partial y^2$$

By way of comparison, the corresponding results for the present computational models are:

Computational Model	$-(\overline{uv})_+/Y^3$ near wall
Model 1	.0007
Model 2	.0005

Of the two damping factors that yield the correct near-wall behavior, the one based on oscillating shear flow yields values of $(\overline{uv})_+/Y^3$ closer to the computational models.

Wall Boundary Condition for Dissipation

In k-ε models, as well as in Reynolds stress models of turbulence, it is necessary to impose a boundary condition on the mean homogeneous dissipation ε at the wall. As summarized by Patel et. al. (1981), three different boundary conditions have been employed in the past:
$\varepsilon_w = 0$, $(\partial\varepsilon/\partial y)_w = 0$, and $(\varepsilon)_w = (\partial^2 k/\partial y^2)_w$, where
$2k = (u'^2 + w'^2 + v'^2)$. As a test of the first two of these, the near-wall behaviour in models 1 and 2 of the mean value ε of the computed space and time-dependent turbulence dissipation

$$[(\frac{\partial u}{\partial y})^2 + (\frac{\partial w}{\partial y})^2 + (\frac{\partial v}{\partial y})^2 + (\frac{\partial u}{\partial z})^2 + (\frac{\partial v}{\partial z})^2 + (\frac{\partial w}{\partial z})^2]$$

is shown in figure 15 in wall variables. It is clear that $\varepsilon_w = 0$ is incorrect (as is well known), and that $(\partial\varepsilon/\partial y)_w = 0$ is also incorrect. That the third boundary condition is a correct one, follows directly from the limiting near wall behavior of u' and w'. Moreover an alternate boundary condition for ε_w that does not involve $\partial^2 k/\partial y^2$, but only a first derivative, can also be derived. We have

Still a different damping factor is obtained from the analogy of oscillating shear flow over an infinite stationary wall (Chapman and Kuhn, 1981). This type of flow seems more analogous to real flows than does the Stokes flow of an oscillating plate under a stationary fluid. In oscillating shear flow the u fluctuations are damped as $D_{os} = (1 - 2\cos\eta\, e^{-\eta} + e^{-2\eta})$, where $\eta \equiv Y/A_{os}$, and A_{os} is a constant. This damping factor applied to Reynolds Stress also yields the correct cubic power-law behaviour near a wall, $-(\overline{uv})_+ = k^2 Y^3/A_{os}$.

In each case the constants A, A_{op}, and A_{os} are determined through a quadrature (Van Driest, 1956) in which it is required that the logarithmic law of the wall for $\overline{U}(Y)$ is satisfied. Using $5.6 + 5.75 \log Y$ for the logarithmic region, the constants that fit this turn out to be $A = 27.8$, $A_{op} = 71.2$, and $A_{os} = 111$. As illustrated in figure 14, the resulting $\overline{U}(Y)$ profiles are nearly the same for all three damping factors. As far as $\overline{U}(Y)$ and momentum decrements are concerned, therefore, it would make relatively little difference which damping factor is used.

Although the different damping factors yield similar results for $\overline{U}$, they yield very different results for $\overline{uv}$ near a wall. For applications involving heat transfer in fluids with high Prandtl number, or diffusion in fluids with high Schmidt number, the near-wall values of $\overline{uv}$ are of central importance. The three different damping factors, when used in the simple eddy-viscosity (mixing-length) model of turbulence, yield the following results for Reynolds stress near a wall:

Damping Factor	$-(\overline{uv})_+/Y^3$ near wall
D_{vd}, Van Driest	.0002 Y
D_{op}, oscillating plate flow	.0022
D_{os}, oscillating shear flow	.0014

APPLICATIONS TO REYNOLDS AVERAGE
TURBULENCE MODELING

The limiting behaviour of turbulence near a wall as defined by the computational models can be applied to strengthen certain aspects of Reynolds average turbulence modeling. Two examples illustrating this are outlined in the paragraphs which follow. One pertains to the damping factors for Reynolds stress in eddy-viscosity models; and another to the wall boundary condition for dissipation in k-ε models and stress-equation models.

Damping Factors For Eddy Viscosity Models

In eddy-viscosity (or mixing length) models, the Reynolds stress near a wall is expressed as $-(\overline{uv})_+ = k^2 Y^2 D$, where $k = 0.4$ is the Karman constant, and D is a "damping factor" required to provide a smooth transition between the wall and the logarithmic region. The most widely used damping factor has been that of Van Driest (1956), namely, $D_{vd} = (1-e^{-Y/A})^2$, where A is a constant. Near a wall this yields $-(\overline{uv})_+ = k^2 Y^4/A^2$, unfortunately, an incorrect limiting behavior. Van Driest obtained his damping factor by using Stokes flow of an oscillating plate under a stationary fluid to obtain $(1-e^{-Y/A})$ as the damping factor for u fluctuations; but he further assumed (incorrectly) that the v fluctuations would be similarly damped, and thus obtained $(1-e^{-Y/A})^2$ as the damping factor for Reynolds Stress.

It is of interest that the correct near wall behaviour of Reynolds stress is obtained if the analogy of oscillating plate flow is adhered to for v as well as u fluctuations. The incompressible v-velocity field for an infinite plate oscillating in the y direction is not damped; hence the damping factor for oscillating plate flow is $D_{op} = (1-e^{-Y/A_{op}})$, where A_{op} is a constant. This yields the correct cubic power-law behaviour near a wall, $-(uv)_+ = k^2 Y^3/A_{op}$.

-35-

(e.g., along the dashed line in the sketch) is such that u and $\partial w/\partial z$ are positively correlated during both of these motions, and hence produce a y^3 term. We conclude from the requirement of mass conservation, therefore, that the leading y^3 term in Reynolds stess is provided by the sweep and ejection motions near a wall for streamwise homogenous or inhomogenous flows. Since these structures are present in flows with or without streamwise pressure gradient, it follows that the limiting $\overline{uv}$ behavior near a wall will in general be proportional to y^3. The constant of proportionality in wall variables is 0.7×10^{-3} for model 1, and 0.5×10^{-3} for model 2.

From the above considerations we can now understand how some previous theories have incorrectly yielded y^4 variations for $\overline{uv}$. Elrod (1957), for example, obtained the y^4 variation for streamwise homogenous flows through the erroneous assumption that ".. by symmetry, u and w (and their derivatives) are uncorrelated." In the Reynolds Stress producing sweep motions, u and $\partial w/\partial z$ are strongly correlated; and this correlation produces a y^3 term. We believe that implicit in the theory of Ohji (1967), which yielded a y^4 variation for $\overline{uv}$, is also some erroneous assumption equivalent to assuming that u and $\partial w/\partial z$ are uncorrelated.

A simple physical explanation based on mass conservation in sweep and ejection motions can be given for Reynolds stress varying as y^3. Very near the wall the leading terms in a Taylor series expansion for the fluctuating velocities are

$$u = f(x,z,t)y + \ldots \qquad\qquad w = g(x,z,t)y + \ldots$$

For mass conservation,

$$- \frac{\partial v}{\partial y} = \frac{\partial u}{\partial x} + \frac{\partial w}{\partial z} = \left(\frac{\partial f}{\partial x} + \frac{\partial g}{\partial z}\right) y + \ldots$$

so that integration yields,

$$- v = \left(\frac{\partial f}{\partial x} + \frac{\partial g}{\partial z}\right) \frac{y^2}{2} + \ldots$$

The leading term in Reynolds stress, upon time averaging, becomes

$$- \overline{uv} = \left(\overline{\frac{1}{2} \frac{\partial f^2}{\partial x}} + \overline{f\frac{\partial g}{\partial z}}\right) \frac{y^3}{2} + \ldots$$

which clearly produces a y^3 term in streamwise inhomogenous flows.

In streamwise homogenous flows $\overline{\partial f^2/\partial x}$ is zero and

$$- \overline{uv} = \overline{f \frac{\partial g}{\partial z}} \frac{y^3}{2} + \ldots = \overline{u \frac{\partial w}{\partial z}} \frac{y}{2} + \ldots$$

from which it is seen that a leading y^3 term will also be present if u and $\frac{\partial w}{\partial z}$, (each of which is proportional to y) are positively correlated near the wall. Sweep events primarily and ejection events secondarily, are the Reynolds-stress producing motions close to a wall. These motions are illustrated in the simplified sketch of a sweep and ejection shown in Figure 13. The spanwise distribution of u and w along a given value of y

References (cont.)

Kim, J. (1984): Turbulence Structures Associated with the Bursting Event. Phys. Fluids, in Press.

Kim, J., (1983): On the Structure of Wall Bounded Turbulent Flows. Phys. Fluids, Vol. 26, No. 8, pp. 2088-2097.

Kim, H. T., Kline, S. J., and Reynolds, W. C., (1971): The Production of Turbulence Near a Smooth Wall in a Turbulent Boundary Layer. J. Fluid Mech., Vol. 50, pt. 1, pp. 133-160.

Kim, J. and Moin, P.,(1984): A Factored Fractional Step Numerical Method for Incompressible Navier-Stokes Equations, NASA TM-85898.

Kline, S. J., Reynolds, W. C., Schraub, P. A., and Runstadler, P. W., (1967): The Structure of Turbulent Boundary Layers. J. Fluid Mech., Vol. 30, Pt. 4, pp. 741-773.

Kovasnay, L. S. G., Kibens, V., Blackwelder, R., (1970): Large Scale Motion in the Intermittent Region of a Turbulent Boundary Layer. J. Fluid Mech., Vol. 41, Pt. 2, pp. 283-325.

Kreplin, H. P. and Eckelmann, H., (1979): Propagation of Perturbations in the Viscous Sublayer and Adjacent Wall Region. J. Fluid Mech., Vol. 95, Pt. 2, pp. 305-322.

Kutateladze, S.S., Khabakhpasheva, E. M., Orlov, V. V., Perepelitsa, B. V., and Mikhailova, E. S., (1977): Experimental Investigation on the Structure of Near-Wall Turbulence and Viscous Sublayer. Proc. Symp. on Turbulent Shear Flows, Penn. State Univ., 1977, pp. 17.13-17.22.

Laufer, J., (1954): The Structure of Turbulence in Fully Developed Pipe Flow. NACA TN 1174.

Laufer, J., (1950): Investigation of Turbulent Flow in a Two-Dimensional Channel. NACA TN 2123.

Laufer, J. and Badri Narayanan, M. A., (1979): Mean Period of the Turbulent Production Mechanism in a Boundary Layer. Phys. Fluids, Vol. 14, p. 182.

Lee, M. K., Eckelman, L., and Hanratty, T. J., (1974): Identification of Turbulent Wall Eddies Through the Phase Relationship on the Components of the Fluctuating Velocity Gradient. J. Fluid Mech., Vol. 66, Pt. 1, pp. 17-33.

References (cont.)

Lu, S. S. and Willmarth, W. W., (1973): Measurements of the Structure of the Reynolds Stress in a Turbulent Boundary Layer. J. Fluid Mech., Vol. 60, Pt. 3, pp. 481-511.

Moin, P., and Kim, J. (1982): Numerical Investigation of Turbulent Channel Flow, J. Fluid Mech., Vol. 118, pp. 341-377.

Moser, R. D. and Moin, P. (1984): Direct Numerical Simulation of Curved Channel Flow. Report No. TF-20, Dept. of Mechanical Engineering, Stanford University.

Moshman, J. (1967): Random Number Generation, Mathematical Methods for Digital Computers, Vol. II, ed. by A. Ralston and H. S. Wilf, John Wiley & Sons, pp. 249-263.

Nikolaides, C. and Hanratty, T. J. (1983): Computer Simulation of the Time Varying Velocity Field in the Viscous Wall Region. Proc. 4th Symposium on Turbulent Shear Flows.

Nychas, S. G., Hershey, H. C. and Brodkey, R. S.,(1973): A Visual Study of Turbulent Shear Flow. J. Fluid Mech., Vol. 61, Pt. 3, pp. 513-540.

Offen, G. R. and Kline, S. J.: A Proposed Model of the Bursting Process in Turbulent Boundary Layers. J. Fluid Mech., Vol. 70, Pt. 2, 1975, pp. 209-228.

Ohji, M. (1967): Statistical Theory of Wall Turbulence. Phys. Fluids Supplement, pp. 5153-5154.

Patel, V. C., Rodi, W., and Scheuerer, G. (1981): Evaluation of Turbulence Models for Near-Wall and Low-Reynolds Number Flows, Proceedings of 3rd Symposium on Turbulent Shear Flows, Univ. Calif; Davis pp. 1.1 - 1.8.

Praturi, A. K. and Brodkey, R. S., (1978): A Stereoscopic Visual Study of Coherent Structures in Turbulent Shear Flow. J. Fluid Mech., Vol. 89, Pt. 2, pp. 251-272.

Rao, K. N., Narasimha, R., and Badri Narayanan, M. A.,(1971): The Bursting Phenomenon in a Turbulent Boundary Layer. J. Fluid Mech., Vol. 48, Pt. 2, pp. 339-352.

Reichardt, H. (1951): Vollstandige Darstellung der Turbulenten Geschwindigkeitsverteilung in Glatten Leitungen Zeit, Angew. Math. Mech. 31, pp. 208-219.

References (concluded)

Schildknecht, M., Miller, J. A., and Meier, G. E. A., (1979): The Influence of Suction on the Structure of Turbulence in Fully Developed Pipe Flow. J. Fluid Mech., Vol. 90, Pt. 1, 67-107.

Schraub, F. A. and Kline, S. J., (1965): A Study of the Structure of the Turbulent Boundary Layer With and Without Longitudinal Pressure Gradients. Stanford Univ. Dept. of Mech. Engrg. Rept. MD-12.

Smith C. R., (1978): Visualization of Turbulent Boundary Layer Structure Using a Moving Hydrogen Bubble-Wire Probe. AFOSR/Lehigh Univ. Workshop.

Ueda, H. and Hinze, J. O., (1975): Fine-Structure Turbulence in the Wall Region of a Turbulent Boundary Layer. J. Fluid Mech., Vol. 67, Pt. 1, pp. 125-143.

Van Driest, E. R. (1956): On Turbulent Flow Near a Wall, J. Aeronautical Sci. 23, pp. 1007-1011.

Wallace, J. M., Eckelmann, H., and Brodkey, R. S., (1972): The Wall Region in Turbulent Flow. J. Fluid Mech., Vol. 54, Pt. 1, pp. 39-48.

Wallace, J. M., Brodkey, R. S., and Eckelmann, H.,(1977): Pattern Recognized Structures in Bounded Turbulent Shear Flows. J. Fluid Mech., Vol. 83, Pt. 4, pp. 673-693.

Willmarth, W. W., (1975): Structure of Turbulent Boundary Layers. Applied Mech. Rev., pp. 159-247.
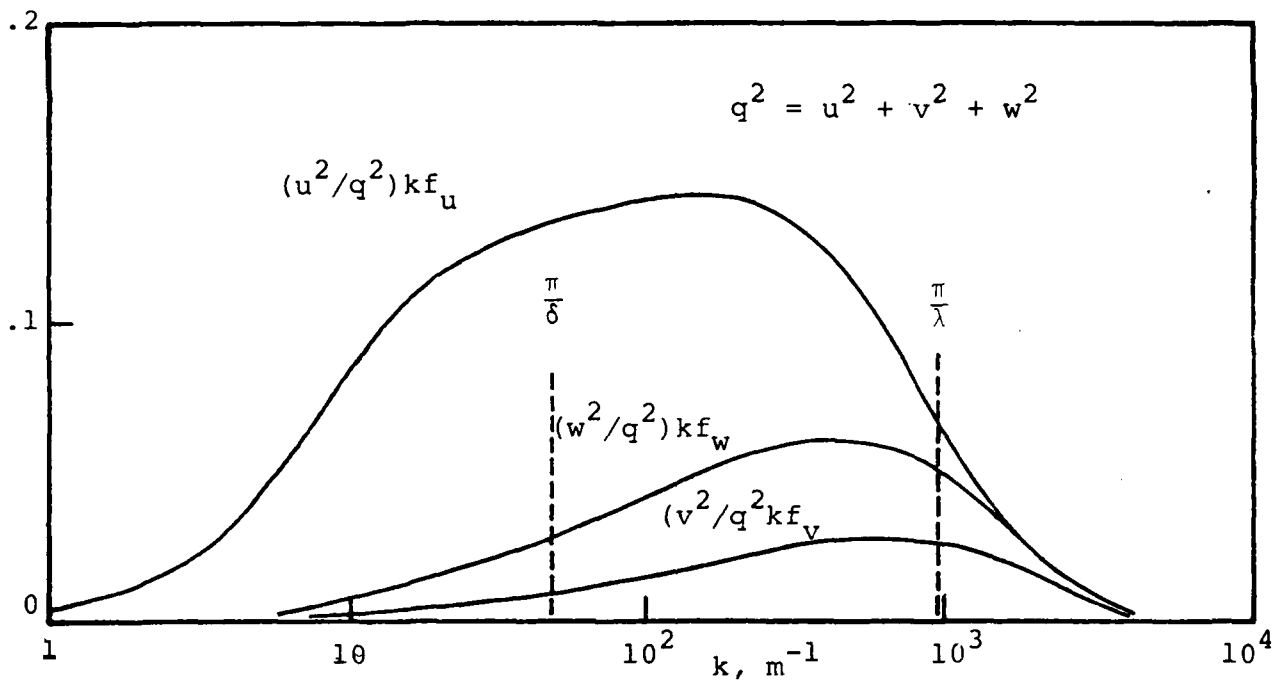
Figure 1. Spectral density of the three components of velocity fluctuation at Y = 40 from data of Fulachier (]972).
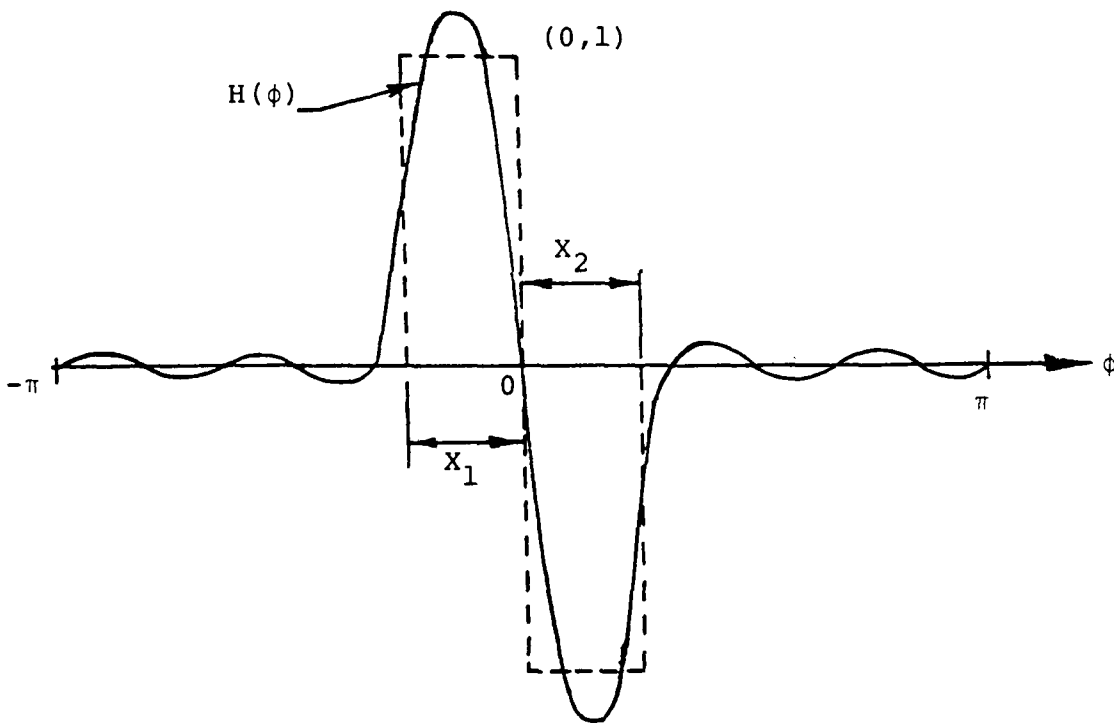
Figure 2. Sketch of truncated Fourier series
approximation to rectangular pulse function.
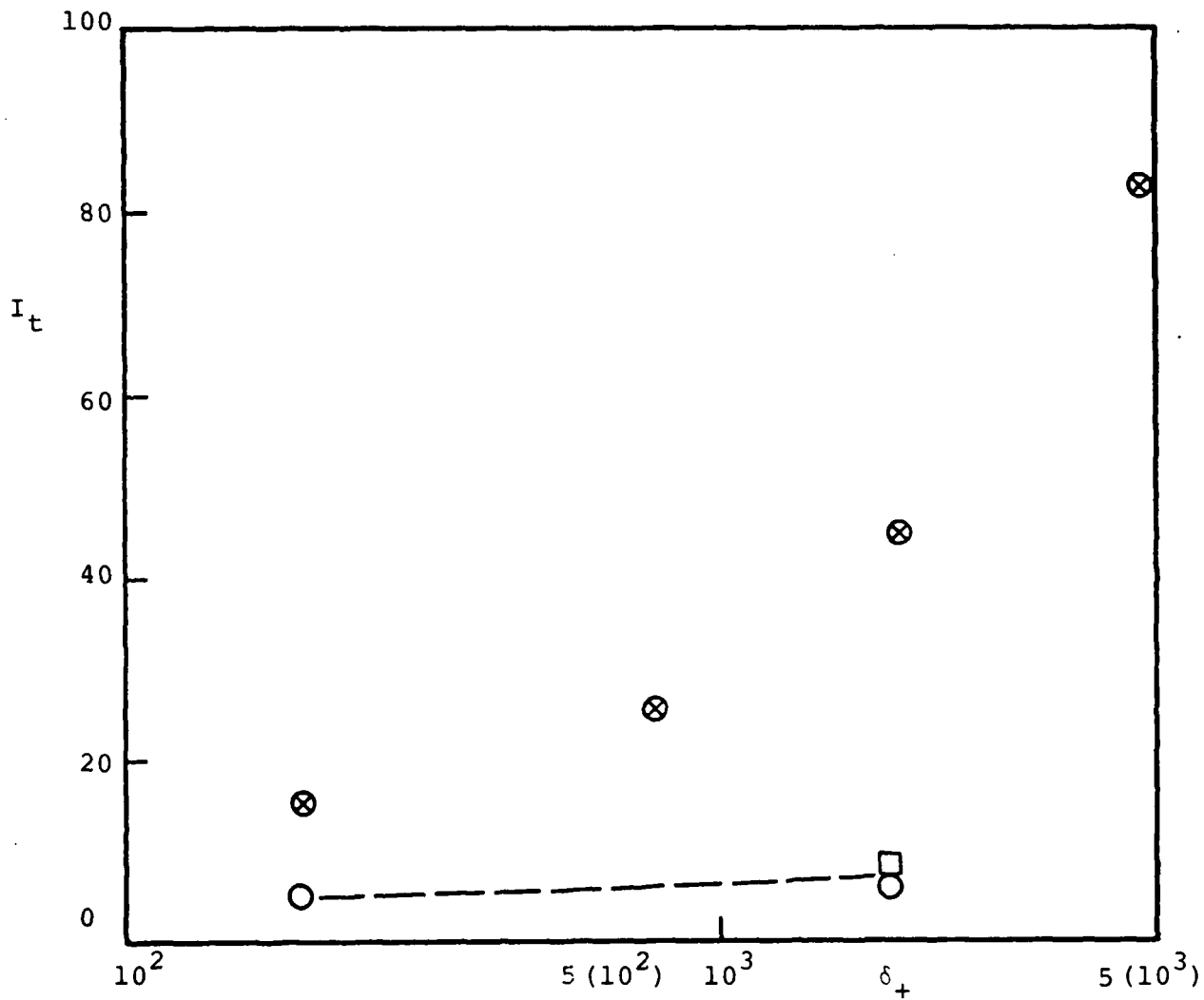
Figure 3. Integral time scale data at outer
edge of Viscous sublayer. ⊗ u,
O v, □ w, from experimental data of
Comte-Bellot (1963), Fulachier (1972),
Elena (1977), and Hofbauer (1978).
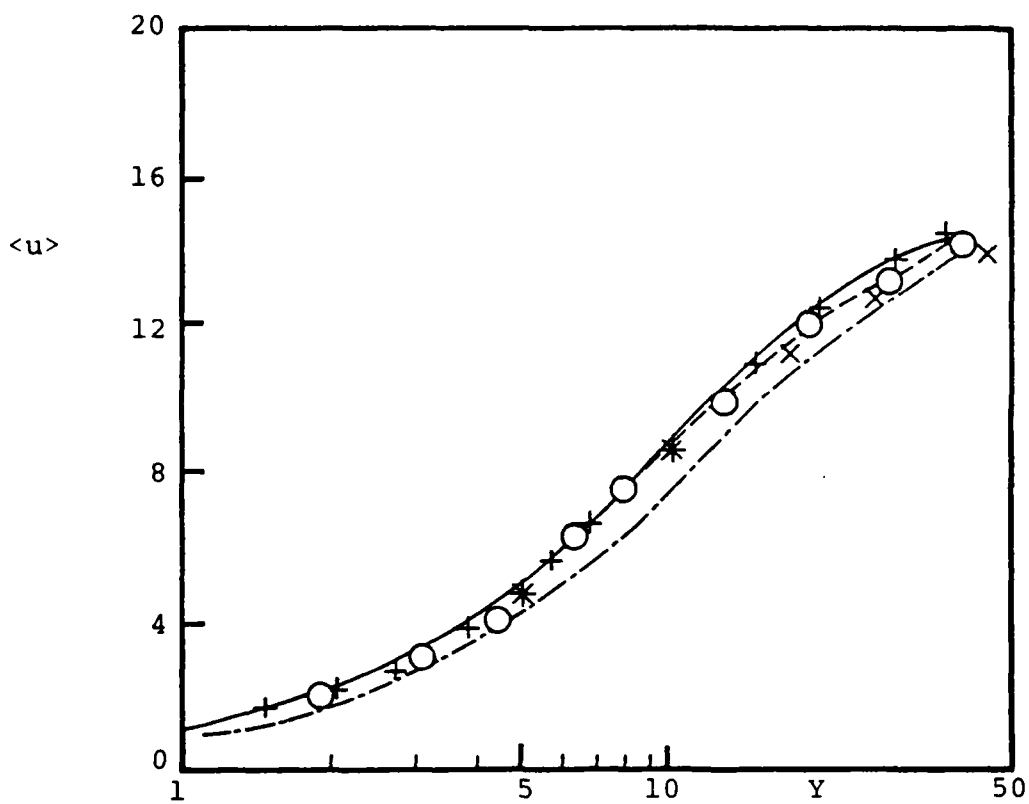
Figure 4. Mean streamwise velocity profiles.

————model 1, ----model 2, ——— – ———model 3,
○Hussain and Reynolds (1975) X Laufer (1954),
+ Ueda and Hinze (1975).
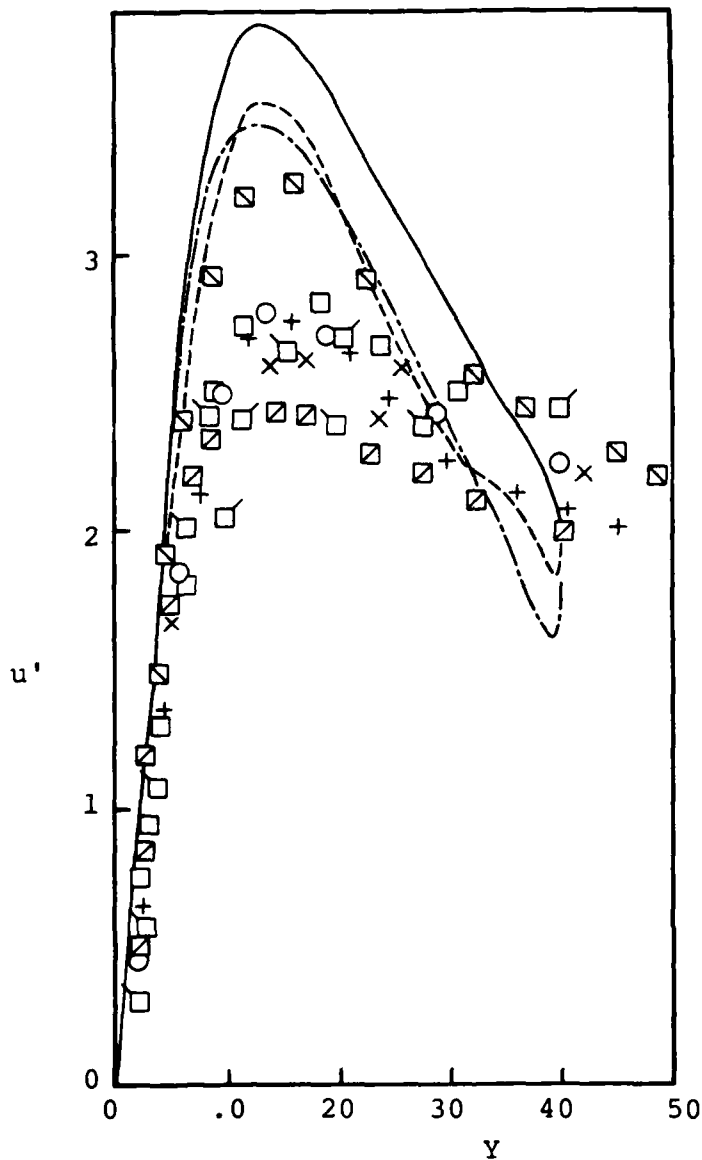
Figure 5. Intensity of velocity fluctuations.

O Schildknecht et. al. (1979), □,◨ Kutateladze
et. al. (1977),
◩ Clark (1968), + Ueda and Hinze (1975), ◳ Laufer (1950),
◨ Hussain and Reynolds (1975), X Laufer (1954)

————— Model 1, ------ Model 2, ——— - ——— Model 3.

-54-
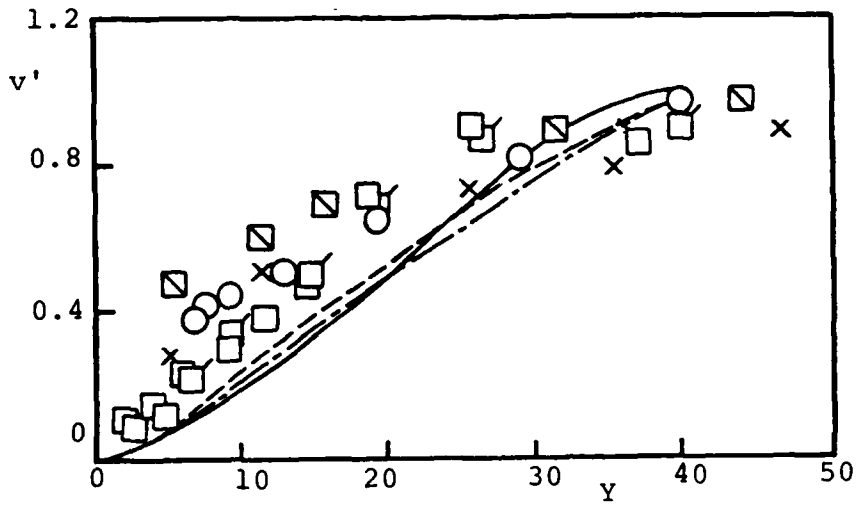
b. v'
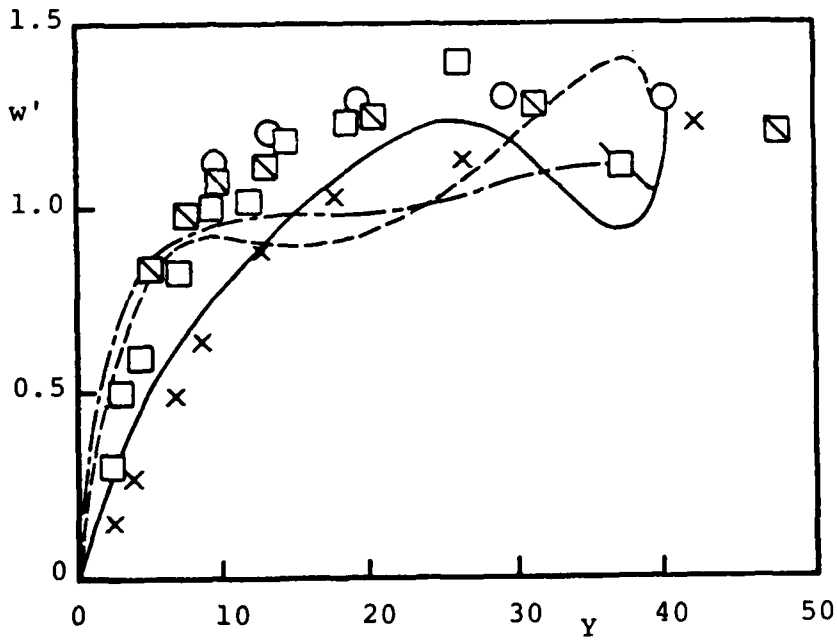
c. w'

Figure 5. Concluded

-55-
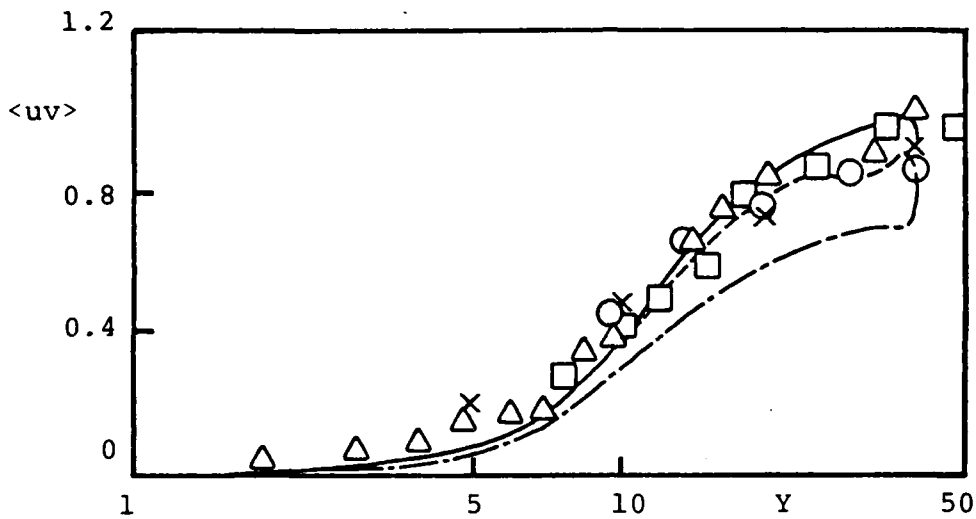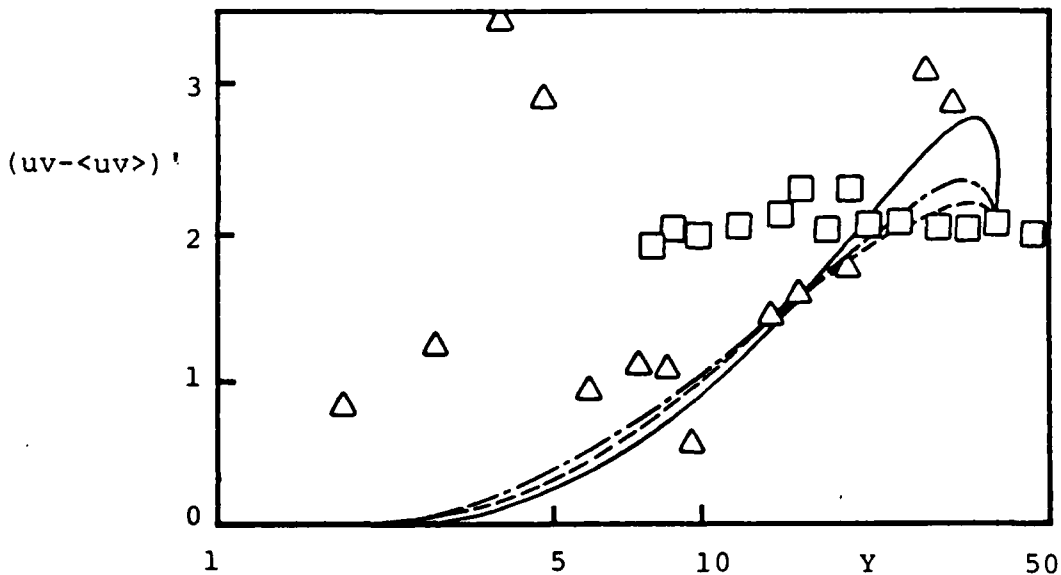
a. Reynolds stress.

b. Intensity of Reynolds stress fluctuations.

Figure 6. Mean Reynolds stress and intensity of Reynolds stress fluctuations. ○ Schildknecht et. al. (1979), △, □ Gupta and Kaplan (1972), X Laufer 1954. ———— Model 1, - - - - - Model 2, ——— - ——— Model 3.
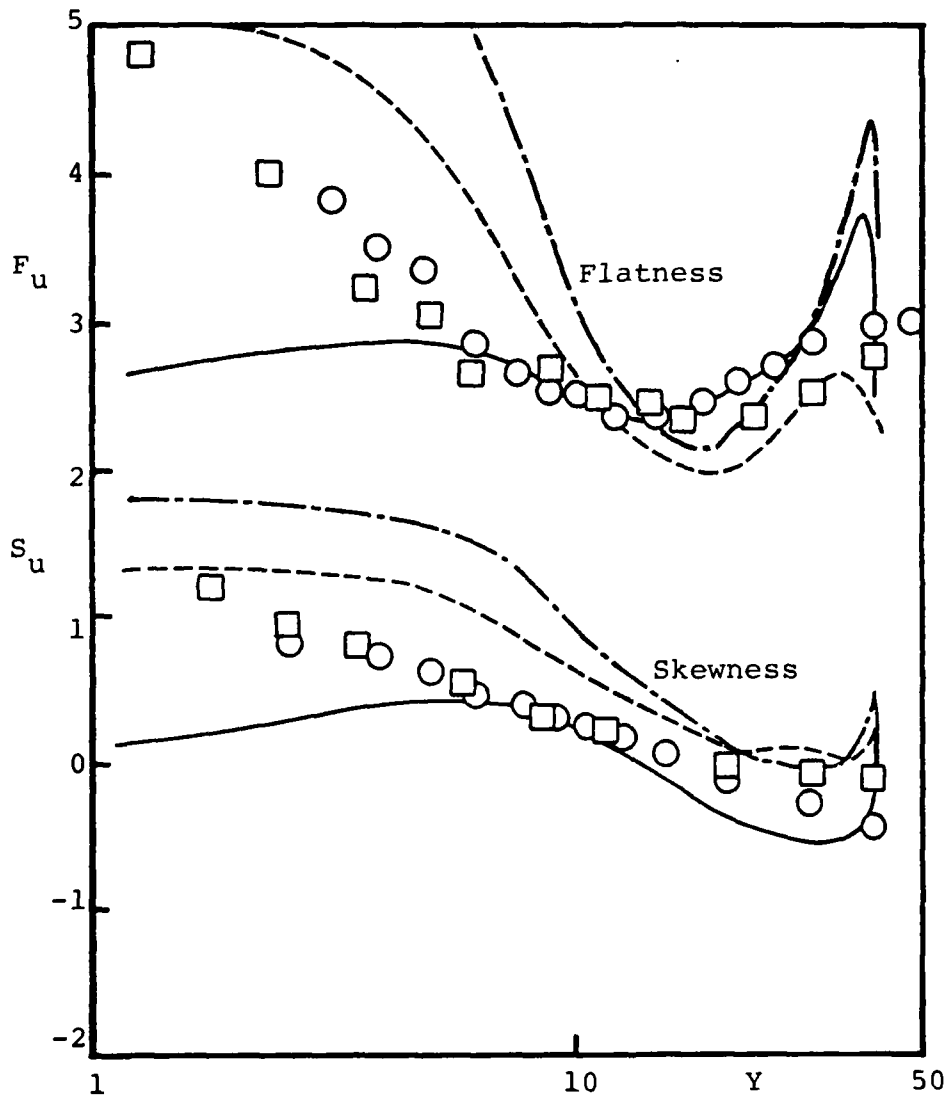
Figure 7. Skewness and flatness of u velocity fluctuations

○ Ueda and Hinze (1975), □ Elena et. al. (1979)

——— Model 1, ----- Model 2, —— - —— Model 3.
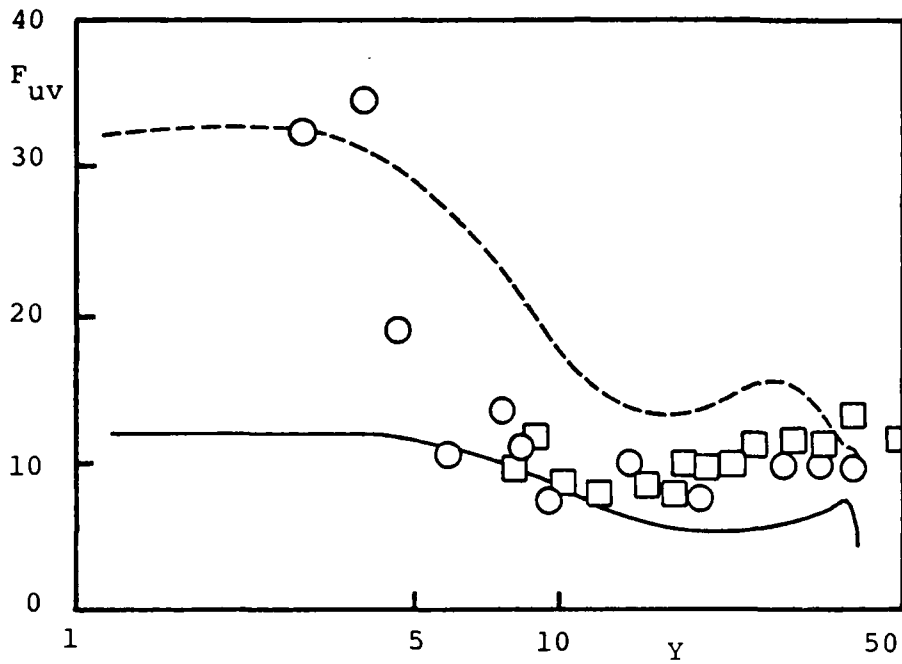
a. Flatness
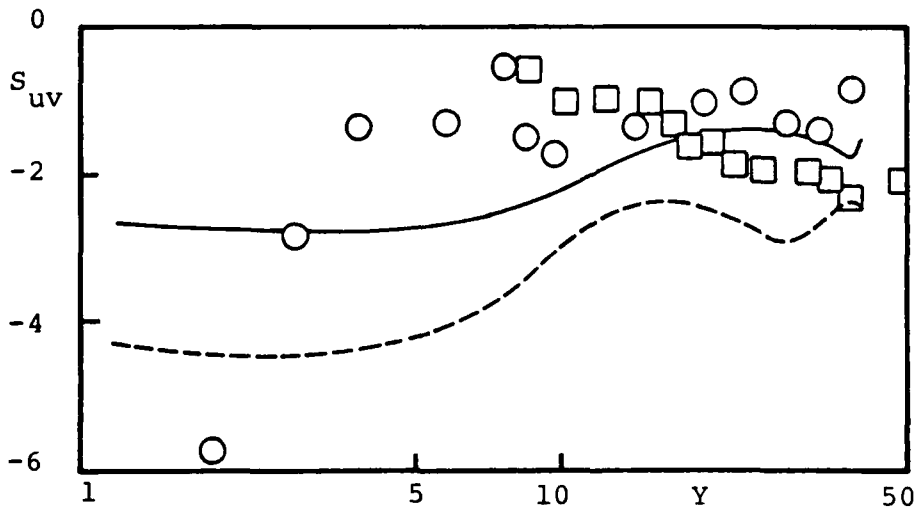
b. Skewness

Figure 8: Skewness and flatness of Reynolds stress fluctuations.

○,□ Gupta and Kaplan (1972).

——— Model 1, —————— Model 2.
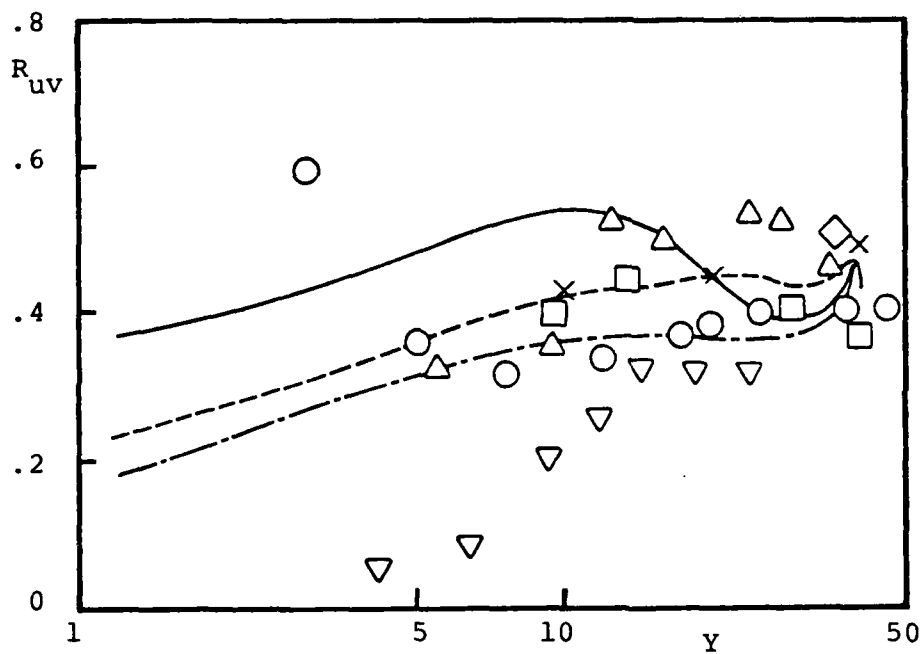
Figure 9:   Reynolds stress correlation coefficients.

  O Eckelmann (1974), △ Kim et al (1968)
  □ Schildknecht et al (1979), ▽ Kulateladze et al (1977)
  ◊ Laufer (1950), X Laufer (1954)
  ———— Model 1, ----- Model 2, ——— - ——— Model 3.
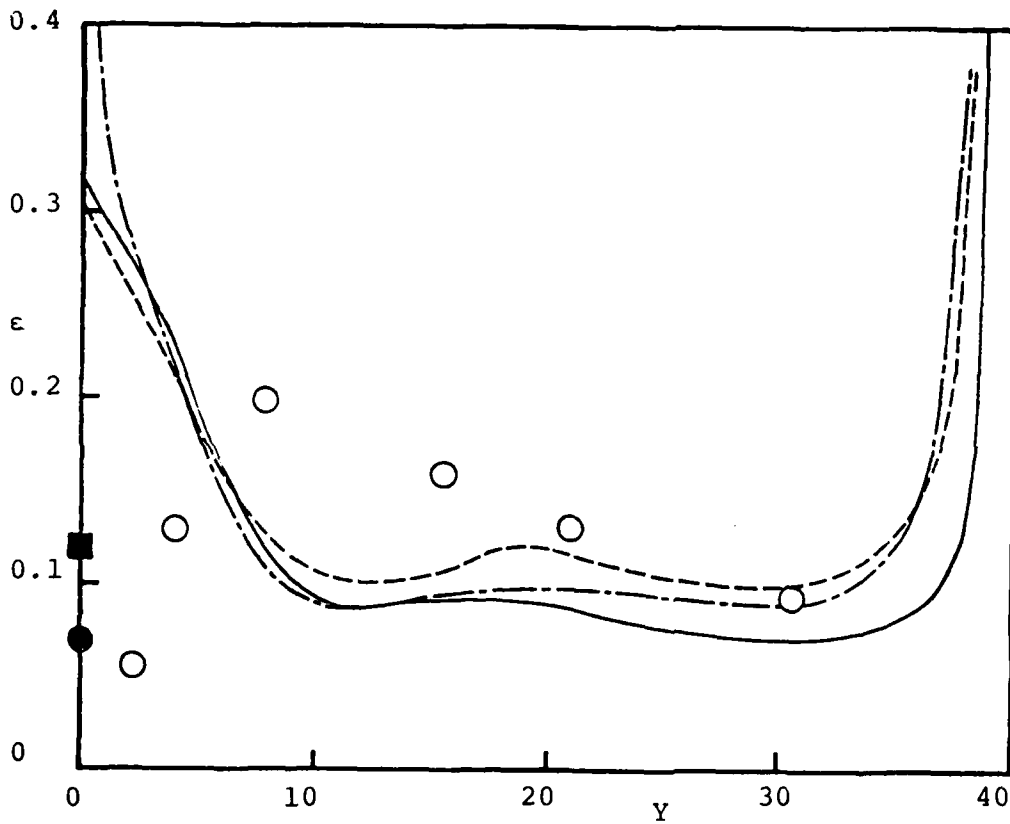
a. Dissipation

Figure 10: Turbulence dissipation and streamwise vorticity fluctuations

○ Laufer (1954), ● Kreplin and Eckelmann (1979), ■ Hogenes and Hanratty (1982)

·———— Model 1, ----- Model 2, ———— - ———— Model 3.
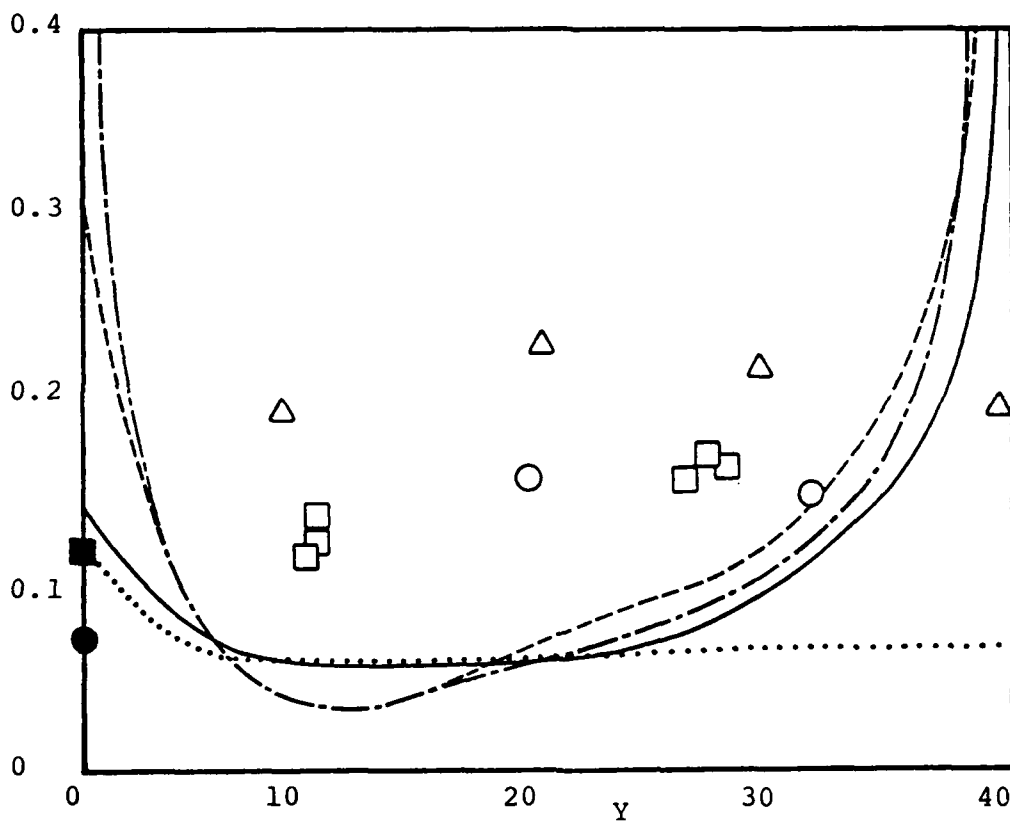
b. Streamwise vorticity fluctuations

Figure 10: Concluded

O Kastrinakas and Eckelmann (1983), □ Kasagi et al (1984)
△ Kastrinakas et al (1975), ● Kreplin and Eckelmann (1979),
■ Hogenes and Hanratty (1982), ... Moin and Kim (1982).
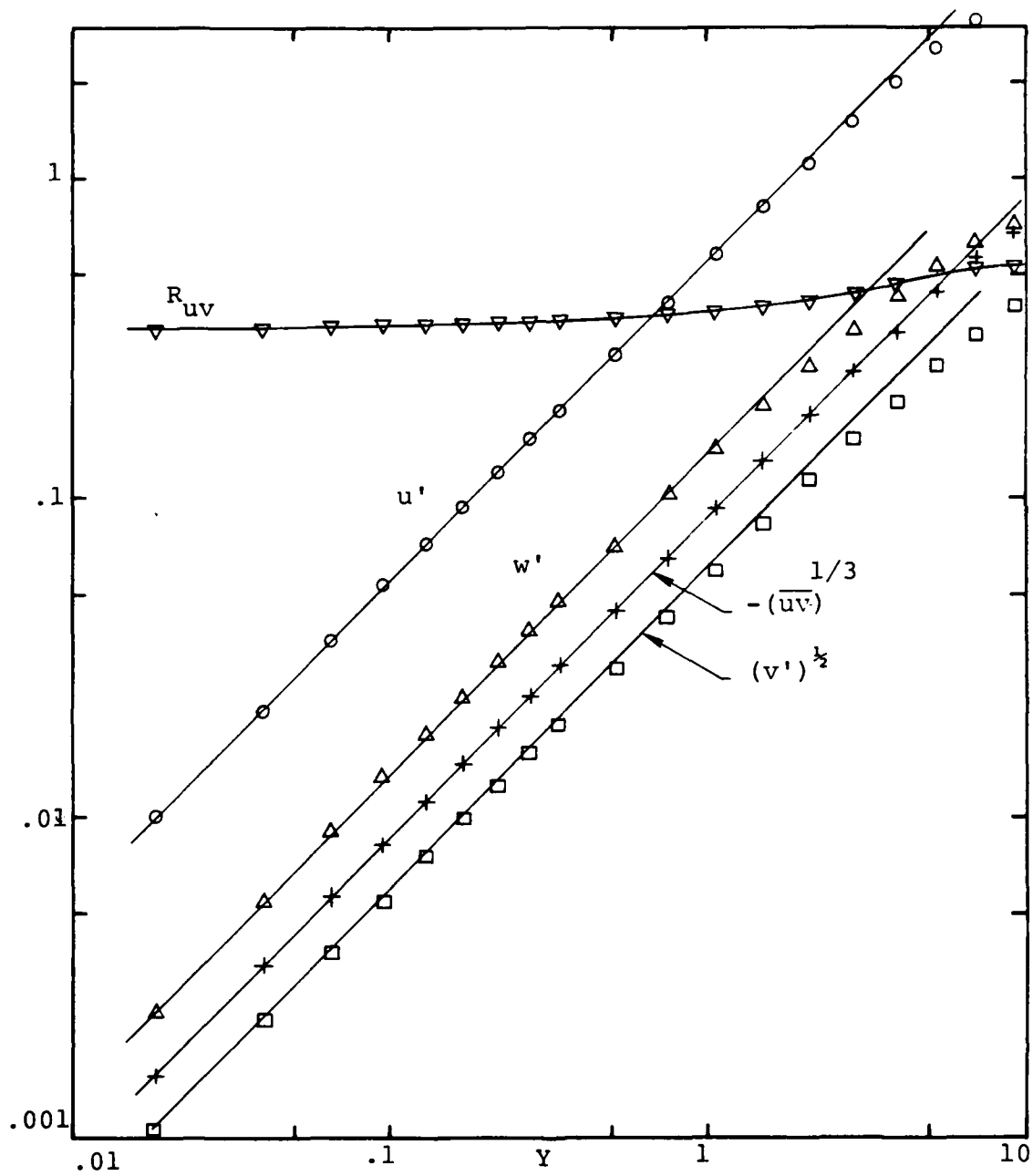
Figure 11. Near-wall behavior of turbulence for Model 1.
$O, u'; \Box, (v')^{\frac{1}{2}}; \triangle, w': \nabla, R_{uv}; +, -(uv)^{1/3}$.
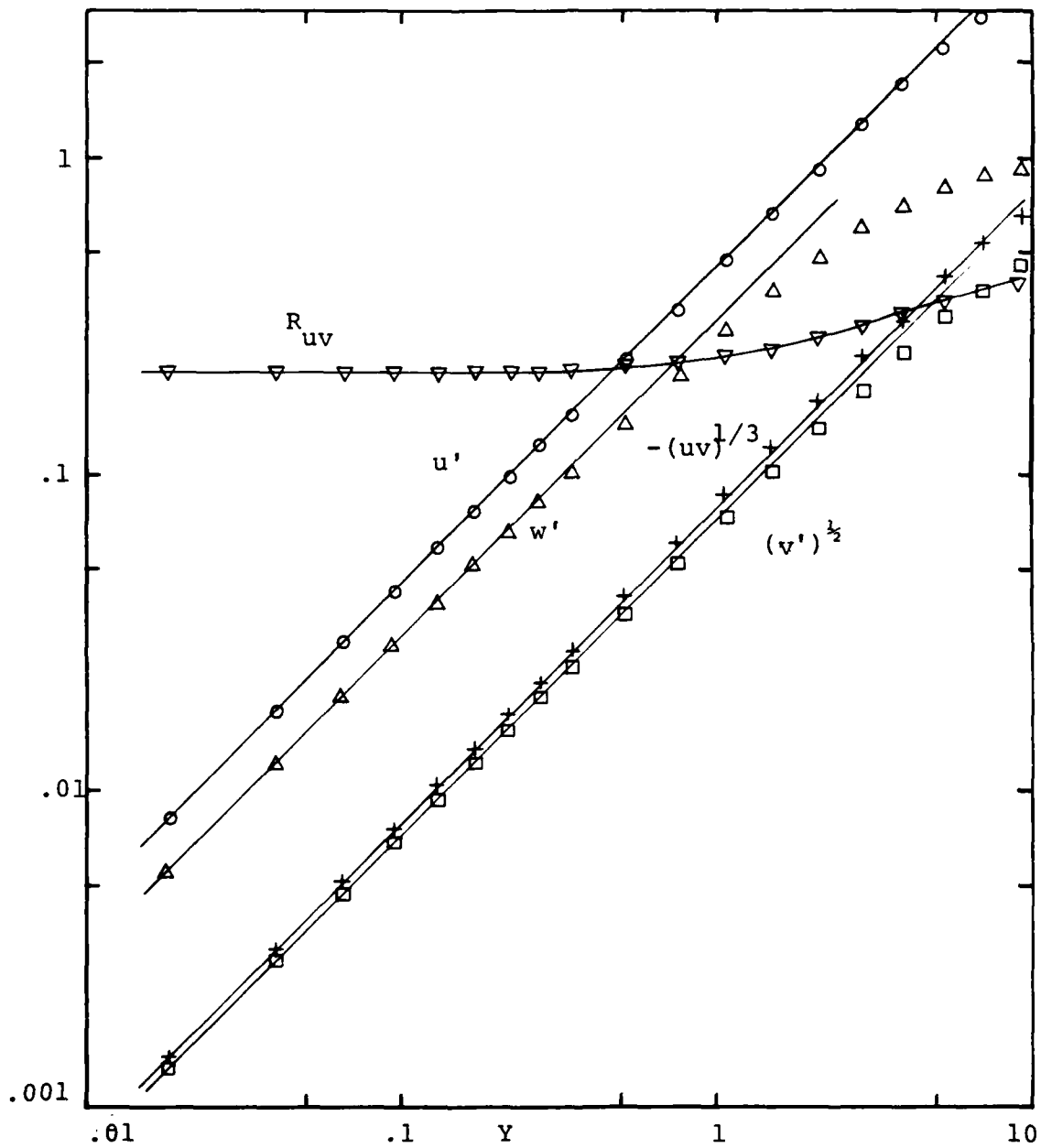Inclined straight lines are proportional to
Y.

Figure 12. Near-wall behavior of turbulence for Model
2: o, u'; □, $(v')^{\frac{1}{2}}$; △, w'; ▽, R_{uv}; +,
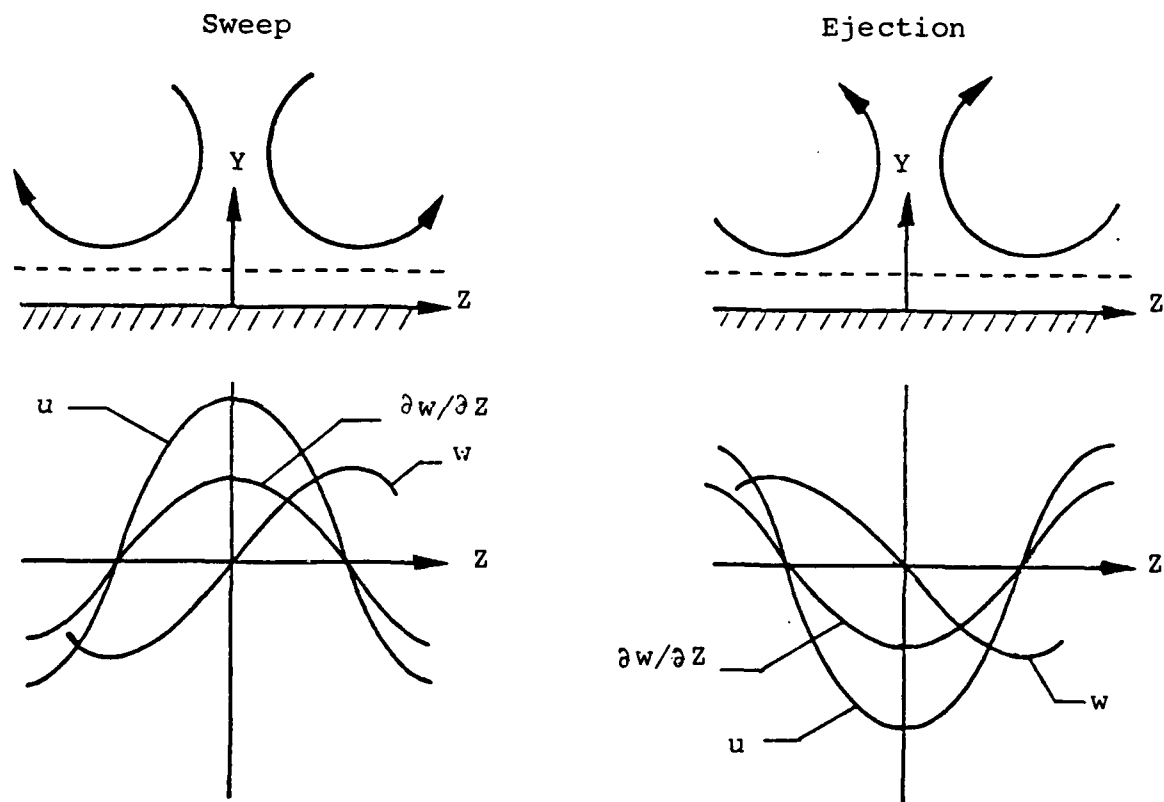$-(uv)^{1/3}$. Inclined straight lines are
proportional to Y.

-63-

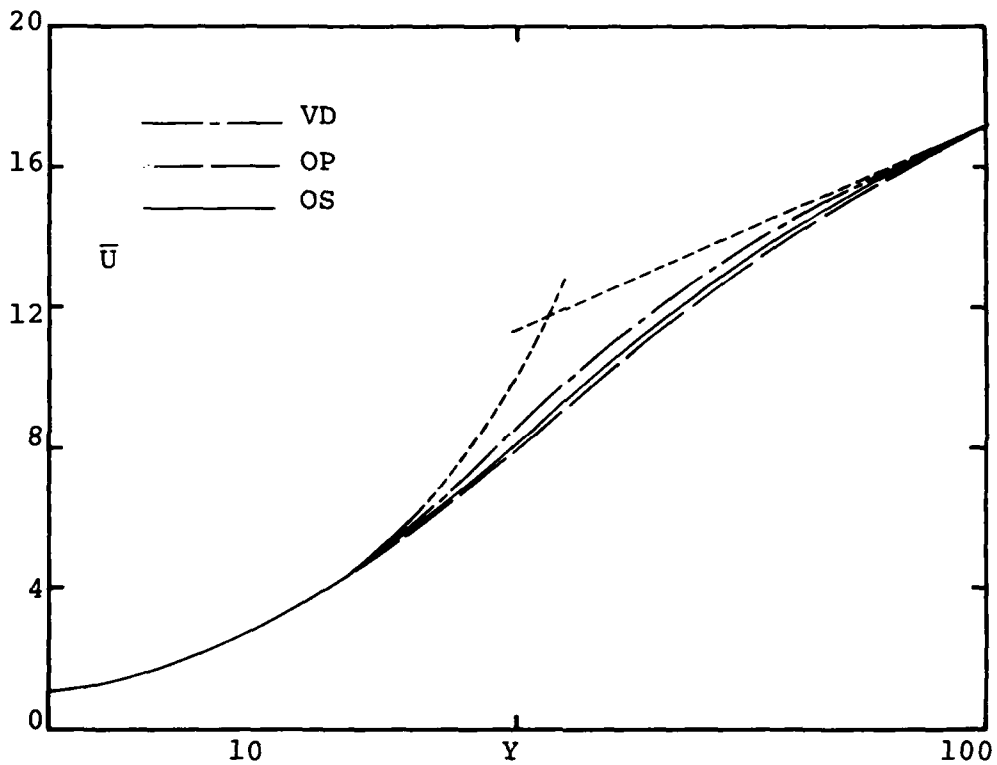Figure 13: Sketch of vortical pair in sweep and ejection motions.

Figure 14. Law of the wall for three different eddy-viscosity damping factors: VD = Van Driest; OP = oscillating plate flow; OS = oscillating shear flow. Short-dash lines: $\overline{U} = 5.6 + 5.75 \log Y$, and $\overline{U} = Y$.
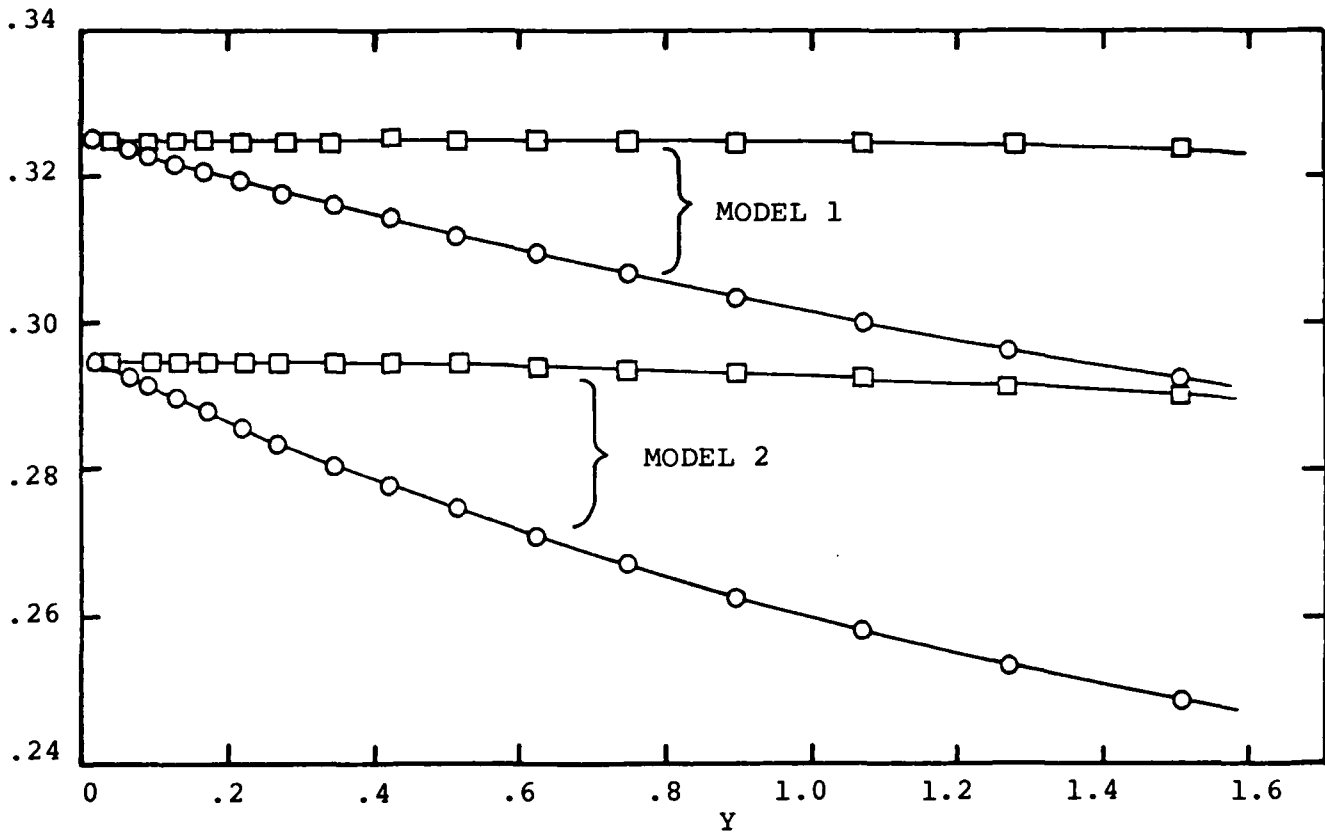
Figure 15: Near-wall behaviour of dissipation ε and the quantity $(\overline{k}-y\partial\overline{k}/\partial y)_{+}$. $\bigcirc = \varepsilon_{+}$, $\square = (\overline{k}-y\partial\overline{k}/\partial y)_{+}$

END

FILMED

4-85

DTIC